



**School of Mechanical and Manufacturing Engineering**

**Faculty of Engineering**

**UNSW Sydney**

**Multi-Objective Optimisation of Stent Designs Focussing on Vessel Calibre**

**BY**

**Roger Lu**

Thesis submitted as a requirement for the degree of Bachelor of Engineering in  
Mechanical Engineering

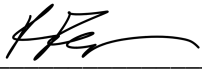
Submitted: 22/04/2022

Student zID: z5207777

Supervisor: Dr Susann Beier (UNSW)

## ORIGINALITY STATEMENT

*I hereby declare that this submission is my own work and to the best of my knowledge it contains no materials previously published or written by another person, or substantial proportions of material which have been accepted for the award of any other degree or diploma at UNSW or any other educational institution, except where due acknowledgement is made in the thesis. Any contribution made to the research by others, with whom I have worked at UNSW or elsewhere, is explicitly acknowledged in the thesis. I also declare that the intellectual content of this thesis is the product of my own work, except to the extent that assistance from others in the project's design and conception or in style, presentation and linguistic expression is acknowledged.'*

Signed  \_\_\_\_\_

Date 22/04/22

### **Abstract**

Percutaneous coronary intervention (PCI) is a common clinical practice, often undertaken to treat the advent of coronary artery disease. Extensive research is being performed in the field to identify and understand which factors contribute to adverse clinical outcomes after implantation, of which stent diameter will be primarily focused upon in this report. FEA and CFD simulations of 19 unique stent geometries were conducted to attain their radial stiffness and WSS results. These were then used to inform an optimisation algorithm to obtain four ideal stent parameters. Overall, key findings suggested that smaller stent diameters were found to be associated with greater radial stiffness values and volume of HWSS. Larger stent diameters were found to be associated with lower radial stiffness values and higher volume of LWSS. Greater material densities also tended to provide stronger radial stiffnesses. For future proceedings, additional simulations for a larger range of diameters and materials should be conducted.

### **Acknowledgements**

I would like to acknowledge my thesis supervisor Susann Beier for understanding, critique and friendliness throughout this thesis. I would also like to thank Ramtin Gharleghi for his prompt responses despite his busy schedule and expertise in FEA and CFD modelling. I would also like to thank Vanessa Luvio for creating invaluable document guides on their past work regarding their comprehensive recommendations, technical procedures, and insightful thesis research. I would also like to thank Deepan Kumar for providing guidance in his research handover, and suggestions in approaching future work. Finally, I would also like to thank Joshua Najdzion for their help in resolving computational issues related to CFD, and guidance in using Katana. Without his reaching out, the set up process of Katana would've proved to be much more confounding.

## Contents

Abstract.....	iii
Acknowledgements.....	iv
List of figures.....	vii
List of tables.....	viii
Nomenclature.....	ix
1. Introduction.....	1
1.1. Coronary Artery Disease.....	1
1.2. Key reasons for failure.....	1
1.2.1. In-stent Restenosis .....	1
1.2.2. In-stent Thrombosis .....	2
1.2.3. Stent Fracture .....	2
1.2.4. Stent under-expansion.....	2
1.2.5. Non-uniform stent expansion.....	3
1.2.6. Adverse Shear Wall Stress.....	4
2. Literature review .....	5
2.1. Key Stent Types.....	5
2.1.1. Bare-metal Stents .....	5
2.1.2. Drug-eluting Stents .....	5
2.2. Targeted Optimisation Objectives .....	5
2.2.1. Mechanical Optimisation Objectives .....	5
2.2.2. Hemodynamic Flow Optimisation Objectives .....	6
2.3. Stent Parameters.....	6
2.3.1. Strut Thickness.....	6
2.3.2. Strut Width.....	7
2.3.3. Stent Length .....	7
2.3.4. Cell Spacing .....	8
2.3.5. Strut Angle.....	8
2.3.6. Connectors .....	10
2.3.7. Strut Cross Section.....	11
2.4. Vessel Calibre .....	11
2.4.1. Oversizing of stent diameters.....	12
2.4.2. Undersizing of stent diameters.....	12

2.5.	Computational Simulations: FEA .....	13
2.5.1.	Model Generation .....	13
2.5.2.	Mesh Generation .....	13
2.5.3.	Material Properties .....	14
2.5.4.	Boundary and Loading Conditions .....	14
2.5.5.	Solution Methodology .....	14
2.6.	Computational Simulations: CFD .....	15
2.6.1.	Mesh Generation .....	16
2.6.2.	Boundary and Loading Conditions .....	16
3.	Methodology .....	16
3.1.	Overview .....	16
3.2.	Stent Geometry .....	17
3.3.	Stent Materials .....	19
3.4.	FEA Set-up .....	20
3.4.1.	Geometry .....	20
3.4.2.	Method .....	21
3.5.	CFD Set-up .....	22
3.6.	Post-processing of results .....	23
3.7.	Optimisation algorithm .....	25
4.	Results and discussion .....	27
4.1.	Multi-objective Optimisation .....	27
4.2.	FEA Results .....	34
4.3.	CFD Results .....	37
4.4.	Discussion .....	39
4.5.	Future Work .....	41
5.	Conclusions .....	42
	References .....	44
	Appendices .....	50
5.1.	Appendix A .....	50

## List of figures

Figure 1 - Percutaneous coronary intervention (PCI) illustrative depiction .....	1
Figure 2 - Foreshortening of the stent (left) [16], dogboning effect (right) [17] .....	3
Figure 3 - General overview of stent strut parameters [25] .....	6
Figure 4 - Example graphic of stent types with stent design labels, depicting cell spacing [28].....	8
Figure 5 - Example of a strut angle orientated at 70° to the hemodynamic flow [32] .....	9
Figure 6 – Stent design nomenclature, example based on a XIENCE PRIME 3.0 mm [39].....	10
Figure 7 - Cross-sectional stent strut geometries with different aspect ratios, AR = width to height (w:h) [45].....	11
Figure 8 - Graphical depiction of coronary circulation.....	12
Figure 9 - Three-point bending test stages [59] .....	15
Figure 10 - Methodology flowchart .....	17
Figure 11 - Boston Scientific Promus ELITE general stent specifications.....	17
Figure 12 - Medtronic Integrity RX stent diameter pressure compliance [66] .....	18
Figure 13 - Stent ID 18, 1.5mm diameter .....	19
Figure 14 - FEA set-up geometry example .....	20
Figure 15 - Simulated contact points of stent during FEA process.....	21
Figure 16 - Displacement boundary condition for FEA set-up.....	21
Figure 17 - Stent cut-out operation on cylinder for CFD set-up .....	23
Figure 18 - Exported Excel data for FEA post-processing .....	24
Figure 19 - Compilation of post-processing results for FEA.....	24
Figure 20 - CFX-Pre conditions for 'sopt1_1.5mm' stent .....	25
Figure 21 - Example output produced by one iteration of the optimisation algorithm.....	25
Figure 22 - Comparison of objectives for '3mm' diameter stent for the non-dominated solutions .....	29
Figure 23 - Comparison of objectives for '3.2mm' diameter stent for the non-dominated solutions .....	29
Figure 24 - Comparison of objectives for '3.7mm' diameter stent for the non-dominated solutions .....	30
Figure 25 - Comparison of objectives for '4mm' diameter stent for the non-dominated solutions .....	30
Figure 26 - Compilation of optimised stent design variations .....	31
Figure 27 - Average radial stiffness distribution among stent diameters.....	34
Figure 28 - Radial stiffness values of varying stent diameters and their material .....	35
Figure 29 - Close-up view of 'Sopt1_1.5mm' .....	35
Figure 30 - Optimised stent deformation geometry and value.....	36
Figure 31 - HWSS and LWSS %Area values of varying stent diameters and their materials.....	37
Figure 32 – Time-averaged wall shear stress distribution along optimised stent geometry .....	38
Figure 33 - CFD output script.....	50
Figure 34 - MATLAB optimisation algorithm UI .....	50

**List of tables**

Table 1 - Mechanical properties of utilised materials .....	19
Table 2 - Compiled optimised results table for 3mm stent .....	26
Table 3 – Initial results table for stent diameters .....	27
Table 4 - Complete optimised results table for all stent diameters .....	32



## Nomenclature

<i>AT</i>	= <i>Alignment Type</i>
<i>BMS</i>	= <i>Bare-metal Stents</i>
<i>CA</i>	= <i>Connector Arrangement</i>
<i>CH</i>	= <i>Cell Height</i>
<i>CoCr</i>	= <i>Cobalt Chromium</i>
<i>CT</i>	= <i>Connector Type</i>
<i>CFD</i>	= <i>Computational Fluid Dynamics</i>
<i>DES</i>	= <i>Drug-eluting Stents</i>
<i>FEA</i>	= <i>Finite Element Analysis</i>
<i>HWSS</i>	= <i>High Wall Shear Stress</i>
<i>ISR</i>	= <i>In-stent Restenosis</i>
<i>IVUS</i>	= <i>Intravascular Ultrasound</i>
<i>LWSS</i>	= <i>Low Wall Shear Stress</i>
<i>MI</i>	= <i>Myocardial Infarction</i>
<i>MSA</i>	= <i>Minimum Stent Area</i>
<i>ND</i>	= <i>Non-Dominated</i>
<i>NP</i>	= <i>Number of Peaks</i>
<i>PCI</i>	= <i>Percutaneous Coronary Intervention</i>
<i>PtCr</i>	= <i>Platinum Chromium</i>
<i>SA</i>	= <i>Intra-strut Angle</i>
<i>SD1</i>	= <i>Stent Dimension 1 (Strut Thickness)</i>
<i>SD2</i>	= <i>Stent Dimension 2 (Strut Width, Rectangular Cross Section)</i>
<i>SF</i>	= <i>Stent Fracture</i>
<i>ST</i>	= <i>Stent Thrombosis</i>
<i>StSt</i>	= <i>Stainless Steel</i>
<i>TAWSS</i>	= <i>Time-averaged Wall Shear Stress</i>
<i>WSS</i>	= <i>Wall Shear Stress</i>
<i>WSSG</i>	= <i>Wall Shear Stress Gradient</i>

# 1. Introduction

## 1.1. Coronary Artery Disease

To tackle the leading cause of death in the developed world – the coronary artery disease, the development of medical stents has been one of the most popular and effective treatments for cure. The source for this disease is known as atherosclerosis, which is the build-up of plaque inside the arteries and the hardening of the blood vessel, causing its passageways to narrow and reducing the flow rate of blood in each vessel. To counteract this contraction process, a procedure known as percutaneous coronary intervention (PCI) can be performed, which involves inserting a small balloon catheter and coronary stent into a patient's arteries, of which the balloon expands inside the vessel to widen it and improve the hemodynamic flow to the heart. The stent acts as a tubular scaffold, and works to physically prop the artery open, reducing its chances of restenosis [1].

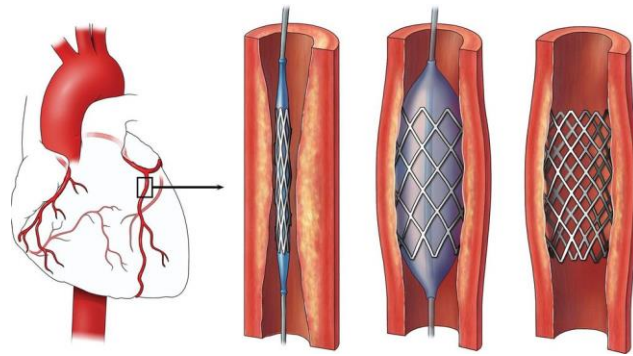


Figure 1 - Percutaneous coronary intervention (PCI) illustrative depiction **Error! Reference source not found.**

## 1.2. Key reasons for failure

### 1.2.1. In-stent Restenosis

However, there are also complications and injuries which may arise from stent implantation, especially the occurrence of in stent restenosis (ISR). ISR is angiographically defined as a  $>50\%$  reduction in luminal area within the stent or in the adjacent native vessel [3] and occurs because of the response of the vascular tissue to the injury caused by coronary angioplasty, known as neointimal hyperplasia [4]. Due to the elastic nature of the arterial walls, they tend to gradually move inwards despite being stretched open with balloon angioplasty. Hence, bare metal stents (BMS), and later drug-eluting stents (DES), were developed to resist this closing tendency, which achieved restenosis rates of 30% and  $<10\%$  respectively [5]. As these incidence rates are sought to be further reduced, experiments targeting the optimisation of stent parameters are being conducted in current research, and they have proven their impact in affecting a variety of adverse clinical outcomes.

### **1.2.2. In-stent Thrombosis**

In-stent thrombosis (ST) involves the thrombotic occlusion of a coronary stent after PCI, which is the formation of blood clots inside the stent [6]. Although rare, the consequences of thrombosis are severe and may result in fatal complications for victims, of which 15 – 30% of patients afflicted die within 30 days of the event. Recently, studies have indicated that despite the reduction of restenosis rates in DES, an increase in ST incidences are produced as a side effect, affecting particularly late stent thrombosis. Several factors that contribute to ST have been recognised, notably smaller final lumen dimensions due to stent malposition and/or under expansion, stent length, persistent slow coronary blood flow and placement of multiple stents [7]. Thus, by optimising certain components of the stent design such as stent diameter, these detrimental factors can be minimised.

### **1.2.3. Stent Fracture**

Coronary stent fracture (SF) is defined as a discontinuation of any part of the stent structure seen on angiogram [8]. It first came into recognition with the advent of the DES due to their statistically significant increased incidences of SF compared to BMS. Despite their infrequencies, they are still recognised as important complications due to the increased rates of ISR, ST and cardiac event rates associated with SF. This is demonstrated in a study by Kuramitsu et al. [9], noting that in the occurrences of SF after DES implantation, patients were associated with an increased risk of ISR, ranging from 15-60%. Furthermore, the majority of available studies have suggested a higher frequency of SF in a particular type of DES, where Chinikar et al. [10] found that more than 95% of their stent fracture cases were derived from the Cypher Stent. Several hypotheses were proposed in response to this, particularly in regards to the interaction between stent and vessel geometry during stent implantation. Due to the geometric distortion imposed on the stent by the vessel, these mechanical forces caused metal fatigue in the stent and increased the likelihood of SF. As such, stent flexibility seemed to be directly linked to the integrity of the stent structure, where stiffer stent designs such as the Cypher Stent were the most susceptible to SF.

### **1.2.4. Stent under-expansion**

Stent under-expansion, as measured through intravascular ultrasound (IVUS), is an important mechanism of DES failure, causing both restenosis and thrombosis. Per a study by Kang et al. [11] It is defined as a minimum stent area (MSA) of less than 5.0-5.5 mm<sup>2</sup>, of which hazardous levels of intimal hyperplasia often occur due to the diminished capacity in the vessel. Fundamentally, the cause of insufficient stent expansion is often due to factors such as the non-compliance of the stent delivery balloon or selecting an undersized balloon model which fail to inflate the stent to an acceptable diameter. However, in a patient-related study conducted by Taherioun et al. [12], nominal stent diameters of less than 2.75 mm were also strong predictors of stent under-expansion, with one third of stents under 2.75mm failing the IVUS criteria for optimum stent expansion. Furthermore, heavily

calcified plaques in vessels have also been shown to restrict the appropriate expansion range of the implemented stent, causing under-expansion of the stent. To minimise the incidence rates of stent under-expansion, post-dilatation with noncompliant balloons may be performed, and have been shown to substantially improve stent expansion and decrease the frequency of suboptimum stent deployment. To ensure the stent delivery balloon was of adequate size, IVUS guidance during the PCI process should be conducted, as this allows for more accurate assessments of vessel size post-angiography.

### 1.2.5. Non-uniform stent expansion

In stent insertion undergoing PCI, the expansion of the stent may be distributed non-uniformly, resulting in the foreshortening or dogboning of a stent and induce vascular injuries and ISR. The process of foreshortening occurs during radial expansion of the stent and causes the axial length to shorten, whilst the dogboning phenomenon is attributed to the ends of a stent opening first during expansion. Both events have been discovered to have significant adverse impacts on clinical outcomes.

In a study conducted by LaDisa Jr et al. [13], data obtained using CFD indicated that foreshortened stents are associated with an increase in area of the luminal surface exposed to low WSS and elevated special WSSG. This was attributed to the misalignment of the foreshortened stents to the direction of blood flow, disturbing hemodynamic factors, and near-wall velocity vectors. As such, these results implicate that the vessel will experience a greater production of neointimal hyperplasia compared to a stent expanded to its intended length, and hence inducing higher rates of restenosis. Dogboning similarly increases rates of vascular injuries, where the sharp edges and hinges of the stent due to poor design can injure the blood vessel during stent implantation [14], increasing rates of restenosis and thrombosis.

In understanding the manifestations of foreshortened and dogboning stents, a study by Lim et al. [15] showed that foreshortening and dogboning were generally more common in stents with closed unit cells connected by straight link structures, and rarer in stents with open unit cells and bend-shaped link structures, such as the MAC Plus stent. Hence, by using a stent composed of broader unit cells connected by bend-shaped link structures may provide better results in minimising the foreshortening and dogboning of stents.

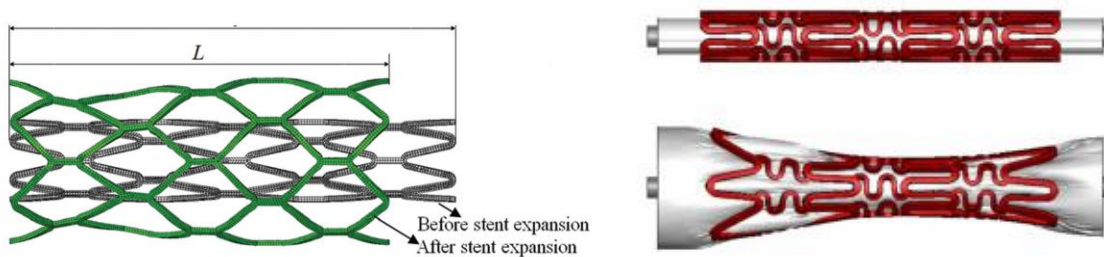


Figure 2 - Foreshortening of the stent (left) [16], dogboning effect (right) [17]

### **1.2.6. Adverse Shear Wall Stress**

#### **Wall Shear Stress (WSS)**

The coronary artery is constantly exposed to mechanical loading in the forms of frictional forces from blood flow and blood pressure. The flow induces WSS in the tangential direction, while blood pressure acts perpendicular to the vessel wall and induces circumferential stresses [18]. Presently, there is no consensus regarding the boundaries which constitute low, intermediate (physiologic), and high WSS – but in general, low WSS is typically represented by  $< 1$  Pa, physiologic WSS as 1-2.5 Pa, and high WSS as  $> 2.5$  Pa. In recent years, investigators have labelled ‘non-low’ WSS (previously known as ‘high WSS’) as physiologic WSS, and high WSS as values higher than physiologic. Based on this classification, researchers have generally associated areas of low WSS and high oscillatory shear spatially with regions of greatest intimal growth following stent implantation. There has also been increasing evidence that high WSS factors contribute to the development of high-risk plaque factors and have been shown in experimental studies to induce specific changes in endothelial migration [19]. However, there still remains inconclusive data linking high WSS to the development of hard clinical events, has been debated as to whether changes in WSS magnitude are the definitive source for atherosclerotic development, or just a consequential effect. Nonetheless, WSS ranges which deviate from physiologic WSS have been shown to produce detrimental clinical outcomes and should still be optimised to restore the WSS to a more physiological range.

#### **Wall Shear Stress Gradient (WSSG)**

The WSSG has historically been defined in literature through the directional derivatives of the WSS and is a representation of the change in WSS over short distances. In complex geometries, high WSS is often accompanied by significant spatial WSSG, which has been shown to cause endothelial migration, disrupted flow, and intimal hyperplasia [20]. Conversely, in a study by Giannoglou et al. [21], low WSSG in combination with low wall pressure gradient were suspected to provoke endothelial cells in providing a mechanism promoting atherosclerosis. However, there is still limited research on the possible detriments of low WSSG.

#### **Time-averaged Wall Shear Stress (TAWSS)**

A description of TAWSS can be summarised as the evaluation of the total shear stress exerted on the wall throughout a cardiac cycle. Low TAWSS values of  $< 0.4$  Pa have been shown to promote atherogenic endothelial characteristics, whilst abnormally high TAWSS values of 15-45 Pa can be thrombogenic [22].

## **2. Literature review**

### **2.1. Key Stent Types**

#### **2.1.1. Bare-metal Stents**

A variety of stent types have been tested historically to reduce the frequencies of such failures, as seen in the introduction of the first type of stent – the bare-metal stents (BMS). First successfully implanted in a human coronary artery in 1986 by Sigwart et al. [23], the BMS demonstrated its superiority over the original angioplasty procedures which were performed without stent deployment, a technique now referred to as plain old balloon angioplasty (POBA). However, these stents still produced a 20-30% incidence of ISR, hence provoking the development of drug-eluting stents to address the problems of ISR encountered with BMS.

#### **2.1.2. Drug-eluting Stents**

While bare-metal stents prevent restenosis by attenuating arterial recoil and contraction, drug-eluting stents (DES) supply an antiproliferative drug to the target lesion that inhibits excessive growth of neointima [24]. In the initial designs of DES, or first-generation DES, they were essentially BMS sprayed with polymer and drugs, using stainless steel as its base material. These designs lowered rates of ISR but were also associated with higher rates of ST than BMS, which encouraged the development of second-generation DES in efforts to improve safety and efficacy. In adopting cobalt-chromium, less toxic antiproliferative drugs and new biocompatible polymer coatings second-generation DES have generally been considered as the superior alternative to BMS, attributed to their lower rates of restenosis and repeat vascularisation [25]. As demonstrated in a patient-level meta-analysis study [24], the primary endpoint of cardiac death or nonfatal myocardial infarction (MI) was lower with newer-generation DES than with BMS (14.5% vs 16.7% respectively). They were also associated with significantly lower rates of target vessel revascularisation (TVR) and definite stent thrombosis.

### **2.2. Targeted Optimisation Objectives**

#### **2.2.1. Mechanical Optimisation Objectives**

In deploying a stent into a damaged artery, its mechanical properties must be determined appropriately to optimise its reliability and utility in treating the respective lesion. The ideal stent has a low profile, is sufficiently flexible to minimise vessel distortion, and exerts sufficient radial force on the vessel wall to overcome lesion resistance and elastic recoil [26]. However, the combined optimisation of all these features is feasibly impracticable, as in optimising one characteristic of stent design, another will often suffer detrimental effects. This can be seen in a study by Wei et al. [27] comparing six stent structures, including three commercially shaped stents and three author-developed stents. The results showed that among the three commercially shaped stents, the Palmaz-Schatz-shaped had the least stent dogboning and recoil but induced the highest von-Mises stress on plaque, arterial intima, and media. Hence, currently available stents are required to compromise between

competing desirable features, resulting in subtle differences in performance characteristics. To produce a stent design which exhibits the aforementioned ideal features, computational simulations of varying attributes of stent parameters should be conducted, in an effort to construct an optimal combination.

### 2.2.2. Hemodynamic Flow Optimisation Objectives

Primarily, the odds ratio of high-risk plaques has been shown to increase at both extremes of WSS and emphasises the importance of minimising the areas afflicted with low and high WSS. As low WSS has explicitly been shown to produce detrimental outcomes, it is commonly accounted for in literature, and is frequently minimised in clinical trials to optimise hemodynamic flow. This is demonstrated in a study by Beier et al. [28] evaluating the impact of the Omega and Biomatrix stent design on WSS, WSSG and TAWSS. In considering relevant parameters including strut spacing, stent size and luminal protrusion, their respective properties were juxtaposed and analysed, highlighting the varying effects of such parameters in influencing the hemodynamic profile.

## 2.3. Stent Parameters

Concerns about the long-term safety of early generation DES induced increased research into other branches of technology, including the optimisation of stent parameters. In designing a stent structure, several parameters must be considered to minimise the chance of failures, to allow for sufficient clearance of hemodynamic flow and to ensure an adequate quality and quantity of mechanical characteristics.

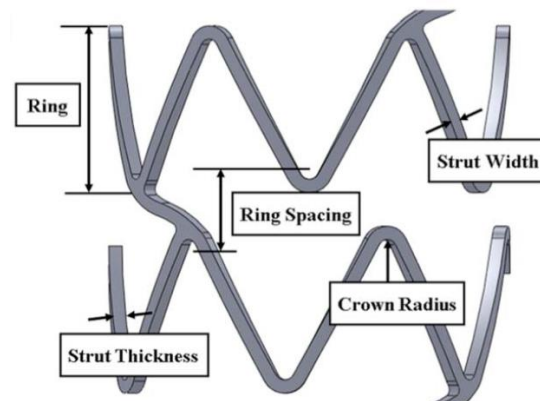


Figure 3 - General overview of stent strut parameters [25]

### 2.3.1. Strut Thickness

The strut thickness is a topic of debate regarding the potential superiority of thinner struts in comparison to thicker struts. The ISAR STEREO 2 study by Pache et al. [29] compared an ultrathin strut (50 $\mu$ m) to a thick

strut (140 $\mu$ m) BMS, where significantly lower incidence rates of clinical restenosis were demonstrated when thinner struts were used. Furthermore, a stratified analysis of pooled randomised controlled trials revealed that thinner-strut DES were also associated with a significant reduction in myocardial infarction (MI) [30]. However, it should be noted that in these designs, there are other differences in design and mechanical properties which might impact on restenosis. Thicker struts tend to have greater radial strengths, and some experimental data suggests that greater hoop strength may cause increased neointimal hyperplasia. As there is still a limited amount of data concerning the overall benefits of thinner struts in DES, research is still being performed to establish a definitive favourite.

### **2.3.2. Strut Width**

A study performed by Kawamoto et al. [31] in 2015 assessed the clinical impact of strut width on periprocedural myocardial infarction (PMI) when treated with bioresorbable stents (BRS) versus first generation sirolimus-eluting stents (SES). The strut width was evaluated by abluminal strut surface area (ASSA), where the average ASSA was higher in BRS samples, and demonstrated significantly higher incidence of PMI compared with SES. As this was first study performed regarding the impact of ASSA on PMI and clinical outcomes at the time, it was inferred that there may be a possible relation between a greater strut width to detrimental clinical outcomes. However, in a study by Pant et al. [32], it was shown that large values of strut width in combination with smaller axial lengths of circumferential rings are optimal in minimising average stresses and maximising drug delivery. This is due to the higher stent width contacting larger areas of the lumen but producing more uniform stresses and delivering higher rates of drug transport into the tissue as a result. Furthermore, by increasing strut width and thickness, radial stiffness and radial length were improved, however coming at the expense of the stent to artery ratio. Thus, the ideal strut width for favourable clinical outcomes is yet to be determined and should be taken into consideration for experimentation in optimising the overall stent design.

### **2.3.3. Stent Length**

Coronary lesions generally consist of a primary flow restricting region and a less severe non obstructive (non-flow-limiting) shoulder region. In a study performed by Mauri et al. [33], they studied whether the stent should cover only the obstructive region of the lesion or be extended to cover the additional unobstructed portion of the lesion. They concluded that the amount of excess stent length increased risk of restenosis independent of the stented lesion length, where each 10 mm of stented lesion length was associated with an absolute increase in percent diameter stenosis of 7.7%, and each 10 mm of excess stent length increased percent diameter stenosis by 4.0% and increased target vessel revascularisation (TVR) at 9 months. Furthermore, as stent lengths are increased, the chances of different failure modes invoked also increase, which is indicated in a study by Kang et al. [34], presuming that there are greater possibilities of stent under-expansion due to the increased length of longer stents. This leads to more severe luminal narrowing and may be the cause of higher restenosis rates in



longer stented lesions. From evaluating this data, longer stent length is seemingly correlated to more adverse clinical outcomes – but further experimentation could be conducted with separate stent parameters to assess an optimal design.

#### 2.3.4. Cell Spacing

The cell spacing (cell height) of stents is a parameter of stents particularly influential to its mechanical integrity and the stress distribution in the artery. This is seen from in the study by Bedoya et al. [21], who determined that from the optimisation of three parameters in eight different designs, increasing the magnitude of axial cell spacing, radius of curvature and amplitude of circumferential rings resulted in lesser stresses in the artery. The benefits of larger cell spacing was also extended to hemodynamic flow, as explored in a study by He et al. [35]. They noticed that the mean axial WSS restoration between struts was higher for stent models with higher inter-strut spacing and allowed for a greater extent of flow restoration in the case of disturbed flows. This idea is further expanded upon in the studies of Beier et al. [28], where cell spacing has also been observed to have a significant effect on hemodynamics. For thicker struts, the adverse effects of low near-wall velocities could be mitigated by greater strut spacing, demonstrating the favourable design impact of greater strut spacing. The inverse of this relation was also found to be true, of which narrower strut spacings were shown to produce areas of adverse low WSS and high WSSG, but were mitigated by adjusting strut size, implicating the importance of balancing multiple design objectives to optimise the stent attributes.

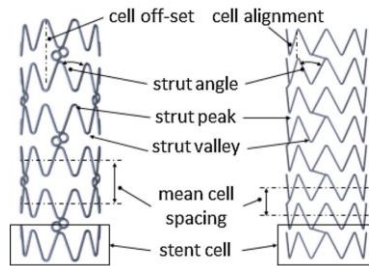


Figure 4 - Example graphic of stent types with stent design labels, depicting cell spacing [28]

#### 2.3.5. Strut Angle

The strut angle, or the orientation of the strut in relation to the principal direction of the blood flow, was found to be significantly important by Gundert et al. [37]. The authors hypothesised that the intra-strut angle was essential in determining the optimal number of crowns in stent design, a parameter which was found to influence the area of low time-averaged wall shear stress (TAWSS). As low WSS is associated with higher restenosis rates, an appropriate strut angle should be determined to minimise such adverse clinical outcomes. As such, they observed that strut angles which were aligned with the flow direction minimised disturbance of blood flow and

decreased the amount of low WSS at the arterial wall. These angles were found to be optimised between 38.5 degrees and 46 degrees for all stent designs, with the angle best minimising the area of low TAWSS observed to be orientated at approximately 40 degrees. However, this result was revised in a later publication by the same authors, who determined that the optimised angle should instead be between 50 and 60 degrees [37]. This was attributed to the discovery that the optimal intrastrut angle was dependent on vessel size, contrary to their previous publication which stated they were independent.

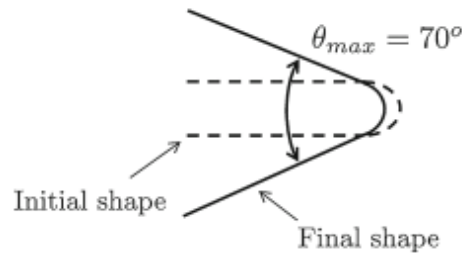


Figure 5 - Example of a strut angle orientated at  $70^\circ$  to the hemodynamic flow [32]

Gundert et al. [37] also established a relationship between stent diameter and the optimal number of crowns for a stent design, proposing that as stent diameter is increased, the number of crowns required would proportionally increase. A larger amount of stent crowns would provide for the greater vessel scaffolding required of larger vessel diameters, but as noted in the study, was also found to cause precarious levels of low TAWSS. However, lowering the amount of stent crowns also came with its respective disadvantages, causing strut and flow misalignment. This finding was coincident with the data collected in a study performed by Beier et al. [28], which similarly implied the detriment of fewer stent peaks in causing flow misalignment. Hence, the optimal number of crowns is still in question, as shown in a study by Iannaccone et al. [38], which found the impact of stent crowns to be minimal in reducing ST and TLR, and that stents with an average number of crowns  $<7.5$  performed similarly to stents with higher average crowns. In this regard, commercial stent designs often use 6 – 9 crowns on average.

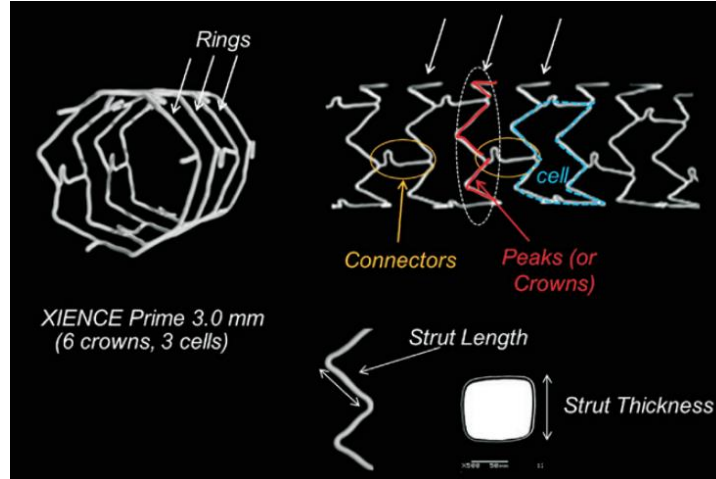


Figure 6 – Stent design nomenclature, example based on a XIENCE PRIME 3.0 mm [39]

### 2.3.6. Connectors

To connect adjacent struts to one another in a stent, segments known as connectors were designed to embody this factor. In its fabrication, many studies have discussed the possible clinical impacts of the number of connectors in a stent, its length, geometry, and alignment with the main flow. This is demonstrated in a study performed by Pant et al. [40], where the connector length in the crossflow direction was found to significantly affect blood flow. In particular, stents with higher percentage of areas exposed to low and reverse WSS were proportionally linked to longer lengths of connectors in the crossflow direction, whereas stents with more parallel configurations, at angles of  $0^\circ$  or  $180^\circ$  to the flow exhibited better clinical outcomes. In regards to connector length, a study by Xiang et al. [41] established a strong connection between a greater number of connectors and beneficial longitudinal stent strength (LSS) results. In analysing a stent with four connectors in comparison to a stent with two, the LSS was found to be nearly three times greater in the former design. The benefits of additional connectors are similarly confirmed by Iannaccone et al. [38] who discovered that stents with an average number of connectors  $>2.5$  was associated with lower ST and TLR. However, in increasing the number of connectors, the flexibility of the stent structure and its adaptability to the vessel is reduced, which is a factor which must be considered when designing stents for curved arteries. Hence, some connector geometries have been modified to adhere to this factor, as discussed by Watson et al. [42], with the Vision and Multi-Link 8 stents encompassing U-shaped loops in its connectors to improve flexibility. The impact of connector geometry was also described in the same study by Xiang et al. [41], which analysed three connector geometries, the L-stent, M-stent, and S-stent. The results indicated that the L-stent exhibited the highest LSS while the S-stent exhibited the lowest.

### 2.3.7. Strut Cross Section

Strut cross sectional shape has been shown across many studies to impose a considerable influence on hemodynamic performance and are modelled either as rectangular or circular. Yongfei et al. [43] performed a relevant analysis by generating six virtual stents with different cross sections within the same ideal arterial model and found that stents with streamlined cross-sectional struts (circular or elliptical arc) were generally superior in comparison to non-streamlined cross-sectional struts (rectangular). Circular and elliptical stents were found to have significantly lower areas of low WSS due to reduced flow disturbances and recirculation zones. Yongfei et al. [43] also observed that when larger aspect ratios were tested on the models, both streamlined and non-streamlined cross-sectional geometries benefitted in low WSS reductions, and hemodynamic flow rate was improved as near-wall velocity was observed to increase. With higher flow rates, this may allow the patient to maintain more cardio intense activities such as running [44]. However, rectangular cross sections are still considered due to their higher surface area and strength, which allows for greater drug delivery to the vessel and capacity to resist buckling, which may result in greater restenosis prevention in the patient. Hence, further investigation into providing the most optimal cross-sectional shape for patient suitability should be considered.

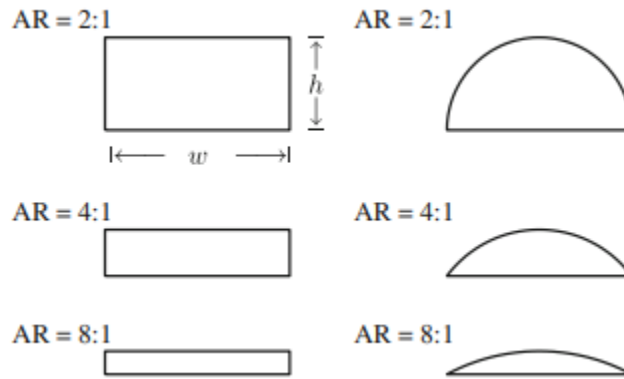


Figure 7 - Cross-sectional stent strut geometries with different aspect ratios,  $AR = \text{width to height } (w:h)$  [45]

## 2.4. Vessel Calibre

The properties and dimensions of coronary arteries are of particular interest when implementing appropriate stents, in which the vessel calibre holds great importance when determining stent diameters. Of a patient-level study performed by Zhou et al. **Error! Reference source not found.**, of 167 study participants, the mean coronary artery diameters among patients were found to be  $2.87 \pm 0.37 \text{ mm}$  for the average diameter,  $4.12 \pm 0.68 \text{ mm}$  for the LM,  $2.26 \pm 0.41 \text{ mm}$  for the LAD,  $2.14 \pm 0.43 \text{ mm}$  for the LCX and  $2.95 \pm 0.6$  for the RCA. No significant differences were found between male and female participants.

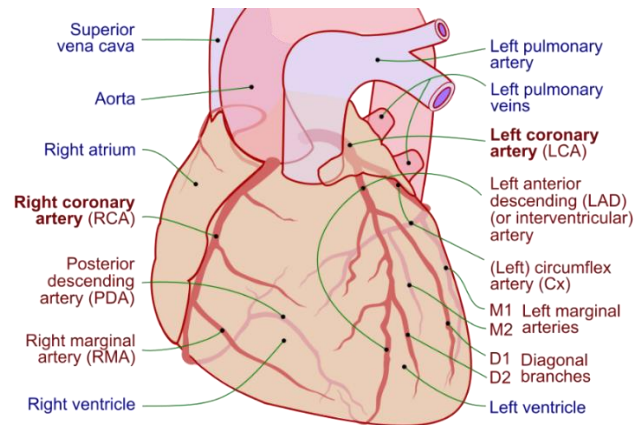


Figure 8 - Graphical depiction of coronary circulation **Error! Reference source not found.**

#### 2.4.1. Oversizing of stent diameters

Stent diameter is a particularly important parameter to be reviewed due to the limited research surrounding its influence in second-generation DES. From a study conducted by Applegate et al. [47], the average stent diameters were found to be  $3.2 \pm 0.5 \text{ mm}$  for BMS stents, and  $3.1 \pm 0.4 \text{ mm}$  for DES stents. As this suggests a general trend of stent oversizing in the commercial industry, a study performed by Kitahara et al. [48] investigated its possible impact, analysing the acute and long term outcomes of DES implantation in de novo coronary lesions. The obtained results indicated that, in particular, smaller vessels treated with smaller stents were associated with greater adverse clinical outcomes. This suggested that, when chosen appropriately, an aggressive selection of larger stents may optimise long term outcomes. The extent to which diameter stents should be sized to is still of consideration, as presented by Stiehm et al. [49]. They performed a series of experiments using three key hemodynamic metrics to evaluate the thrombosis risk of coronary stents and scaffolds, to which the results suggested that bulky stents implanted in small calibre vessels may substantially increase the thrombosis risk.

#### 2.4.2. Undersizing of stent diameters

Many studies have been associating smaller stent diameter with worse long-term outcomes. This can be observed in an examination conducted by Plitt et al. [36], where major adverse cardiovascular events (MACE), TVR, and target lesion revascularisation were all markedly lower in patients with larger stent diameters ( $>3.5 \text{ mm}$ ) compared to smaller stent diameters ( $<2.5 \text{ mm}$ ). As patients with smaller vessel diameters require smaller stent diameters, these negative clinical outcomes are likely to be associated to this correlation, as noted by Gundert et al. [37], where rates of restenosis are significantly higher in patients with smaller diameter vessels ( $< 2.6 \text{ mm}$ ) as even a small amount of neointimal growth can restrict blood flow in the artery. By further narrowing the small vessels with an implantation of another layer of stent struts, this may cause treatment of ISR to be more damaging

than beneficial. As such, to avoid the physical presence of an implantation, additional technologies such as drug-coated balloons (DCB) have been developed to attempt to replace the implantation of a stent while still delivering the necessary drug into the vessel walls, but the incidence for MACE thus far have been similar in both groups (7.5% for DCB, 7.3% for DES) [35]. Hence, as current research has not identified a viable alternative to stents, or established an ideal stent diameter, further research needs to be conducted in the optimisation of this parameter.

## **2.5. Computational Simulations: FEA**

Finite element analysis (FEA) is an important tool in the field of biomedical engineering and is used liberally for the analysis for medical devices such as coronary stents due to their highly variable performance characteristics. FEA works by approximating solutions for systems of differential or integral equations applied over the domains of the inputted geometry. These domains are then broken down into a number of smaller domains, each containing a series of control points known as nodes, and hence allowing specific areas of the model to be analysed [50]. Originally, the entire process of designing, manufacturing, and testing stents would have to be reiterated continuously until satisfactory stent performance was obtained. This could take days to weeks for completion, which is time-consuming, costly, and inefficient. For this reason, FEA and CFD have become increasingly important tools in providing rapid evaluation of stent performance and insight into optimal parameters of stent design [52]. A typical FE analysis of stent deployment involves the following pre-processing stages; the generation of suitable solid models, the generation of FE meshes, the material properties, the boundary and loading conditions, and final solution methodology.

### **2.5.1. Model Generation**

The stent model generation process is often streamlined during commercial stent production, as models are imported from a number of stand-alone computer-aided design packages. It is imperative to ensure an optimal model generation process when performing FEA, as this will lead to more accurate and detailed outcomes in producing stent stress and deformation results, and hence provide more reliable clinical information.

### **2.5.2. Mesh Generation**

Due to the complexity of most stent geometries and strict patent claims of commercial stents which inhibit the distribution of their geometric information, the generation of accurate FE meshes for stents are difficult. In a study proposed by Martin et al. [53], a few strategies were suggested to develop the FE mesh of a stent model. By cutting a physical stent along its longitudinal axis and measuring important geometrical properties using a microscope, these measurements can then be used to define planar stent geometry within an FE package. Another strategy suggested involved the use of X-ray tomography to directly generate a 3D model of the stent, allowing

for a detailed and accurate generation of a complex stent design. For simpler FE mesh definitions, a study by Schiavone et al. [54] was shown to implement fully integrated linear hexahedral elements when analysing their stent and arterial model, as it was found to be suitable in accommodating large bending deformation of the stent during expansion. Santis et al. [55] further elaborated on this method, indicating that to prevent failure and resorting to an unstructured tetrahedral mesh, a multi-block grid is fitted inside the vessel volume, at a distance from the lumen surface. Then, a series of layers are projected from the surface of the grid onto the lumen surface to simulate the vessel wall. The structured hexahedral element type was also consistent with the findings of Azaouzi et al. [56], who also applied a mesh size of 25  $\mu\text{m}$  for the stent, as it was believed to provide a good balance between accuracy and efficiency.

### **2.5.3. Material Properties**

Most recent stent designs utilise the same assortment of material types due to their suitable mechanical and hemodynamics characteristics. In a paper by Thrinayan et al. [57], four different materials were evaluated in regards to their mechanical strengths: stainless steel (SS), platinum chromium (PtCr), cobalt chromium (CoCr) and nitinol. Results comparing these materials showed that L605 and MP35N cobalt chromium experienced the least deformation, strain, and stress results, with the L605 model outperforming the MP35N model in deformation and strain, however experiencing more stress. Both models are commonly tested in studies, with the MP35N model used by Martin et al. [53] and the L605 model used by Hsiao et al. [58].

### **2.5.4. Boundary and Loading Conditions**

As the stent is symmetric along its longitudinal axis, symmetric boundary conditions may be used to minimise computational time. This is reflected in the work by Eshgi et al. [59], in which only a quarter of the model was used to simulate the expansion process. To properly define the symmetry condition, all the nodes perpendicular to the y-axis were restricted to move through the y-axis, and all the nodes perpendicular to the x-axis were restricted to move through the x-axis. In addition, only the movement in the radial direction was permitted for the nodes located at the two ends of the vessel. Lally et al. [60] also defined the stent to be restrained at one node in the circumferential direction to prevent rigid body rotation.

### **2.5.5. Solution Methodology**

#### **Stent Expansion**

In simulating the process of stent expansion during after PCI, a study by Umer et al. [61] generates the radial displacement by applying pressure on the inner surface of the stent, utilising a smooth time step of 2.5 seconds. A pressure of 1.5 MPa was applied for 2 seconds, which was then held constant for 0.2 seconds and subsequently reduced to -0.01 MPa at the end of the time step to allow for elastic recoil.

### **Stent Radial Strength**

To measure the radial strength of the stent, the process is reflected through a study by Hsiao et al. [58], in which an outer cylinder was added to the outside of the stent to simulate the radial strength testing. This cylinder was meshed with surface element (SFM3D4), and works by compressing the stent, forcing it to crimp down to a smaller size. The reaction forces experienced in the radial direction would be analysed as the simulation progressed in time steps. Hoop strength was defined as the maximum value of the total reaction forces during compression, and stent radial strength was defined as the hoop strength divided by the total stent length.

### **Stent Bending Flexibility**

One study by Wang et al. [62] simulated the bending flexibility of coronary stents by performing a three-point bending test on the stent. The setup comprised of one cylindrical load applicator on top of the middle section of the stent, supported by two identical static supports at the ends of the stent. This was split up into two steps – a loading step and an unloading step respectively. In step one, a downward displacement of an upper loading displacer was performed, which would be subsequently returned to initial conditions in step two. Thus, the corresponding reactive forces and displacement values can be obtained to derive the bending stiffness of the stent and quantify its flexibility.

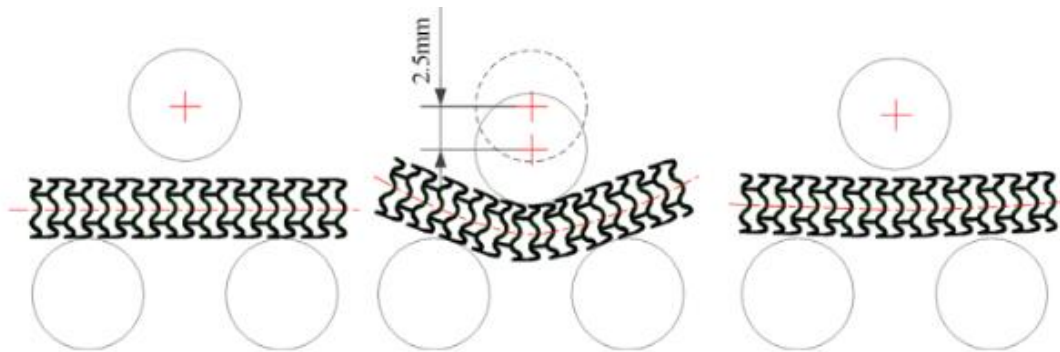


*Figure 9 - Three-point bending test stages [59]*

## **2.6. Computational Simulations: CFD**

Computational fluid dynamics (CFD) is an invaluable tool in analysing the hemodynamic effects of stent geometry, as many of its associated parameters such as pressure, velocity and WSS are difficult to measure in vivo. When a stent is deployed within an arterial lumen, many unexpected flow patterns may be created – and accurately representing such flow conditions generally requires computational methods. As such, CFD is well suited to quantifying the internal incompressible flow conditions, detailing velocity profiles and hemodynamic behaviour throughout the implantation process. The CFD process typically utilises the same model geometry as in an FEA process, but often require the mesh and boundary conditions to be adjusted due to different geometrical sections of interest.



### **2.6.1. Mesh Generation**

The most commonly adopted mesh style for CFD analysis of the stented artery is an unstructured tetrahedral mesh (Lotfi et al. [63], Beier [28], Gundert et al. [37]). A detailed process is provided by Lotfi et al. [63], in which the tetrahedral mesh is developed uniformly along the whole artery, with adaptive tetrahedral or polyhedral grids adding local refinement toward the stent struts – attributed to their high levels of WSSG. In the predominant flow direction, it was noted that the unstructured elements were aligned poorly, hence requiring higher-order prismatic or hexahedral elements on the surface near the wall boundary and at the core of the artery.

### **2.6.2. Boundary and Loading Conditions**

In a study conducted by Lotfi et al. [63], the arterial walls were assumed to be rigid and nonporous, and a no-slip condition was imposed. These conditions were similarly reflected in a study by Hsiao et al. [58], in which blood was defined as incompressible, homogenous, and laminar, with a density of  $\rho = 1060 \text{ kg/m}^3$ . In considering blood as a Newtonian or non-Newtonian fluid, some studies have defined blood as a Newtonian fluid when analysing larger vessel diameters or to simplify computational analysis, as seen in the paper by Lotfi et al. [63]. However, in most stent geometries, a non-Newtonian flow should be considered, as suggested by Mejia et al. [64], as they were shown to have a non-negligible effect on WSS levels. In assigning boundary limitations, Thrinayan et al. [57] would designate the wall regions of the artery as ‘wall’, setting its velocity to zero. For the inlet boundary conditions, blood flow is sometimes modelled with steady state flow conditions for simplicity. However, to accurately replicate biological conditions, the blood flow should be defined as cyclic and pulsatile. These were quantified as a peak velocity of 0.5 m/s and a minimum velocity of 0.1 m/s by Thrinayan et al. [57], resulting in an average velocity of 0.3 m/s. Outlet boundary conditions have been generally categorised as statically constant pressures, with some sources defining them as zero (Lotfi et al. [63]) and others deriving them from systolic and diastolic pressures (Thrinayan et al. [57]), which produces approximately 100 mmHg of blood pressure.

## **3. Methodology**

### **3.1. Overview**

This thesis will be primarily focused on determining the optimal stent diameter through the use of computational modelling software, incorporating ANSYS, MATLAB and Microsoft Excel. In analysing the results obtained, a deepened understanding of the benefits and drawbacks of differing stent diameters may be achieved, which may lead to greater medical and commercial success in coronary stent implantation. To illustrate the processes involved in conducting the analyses, a flowchart is depicted below in Figure 10.

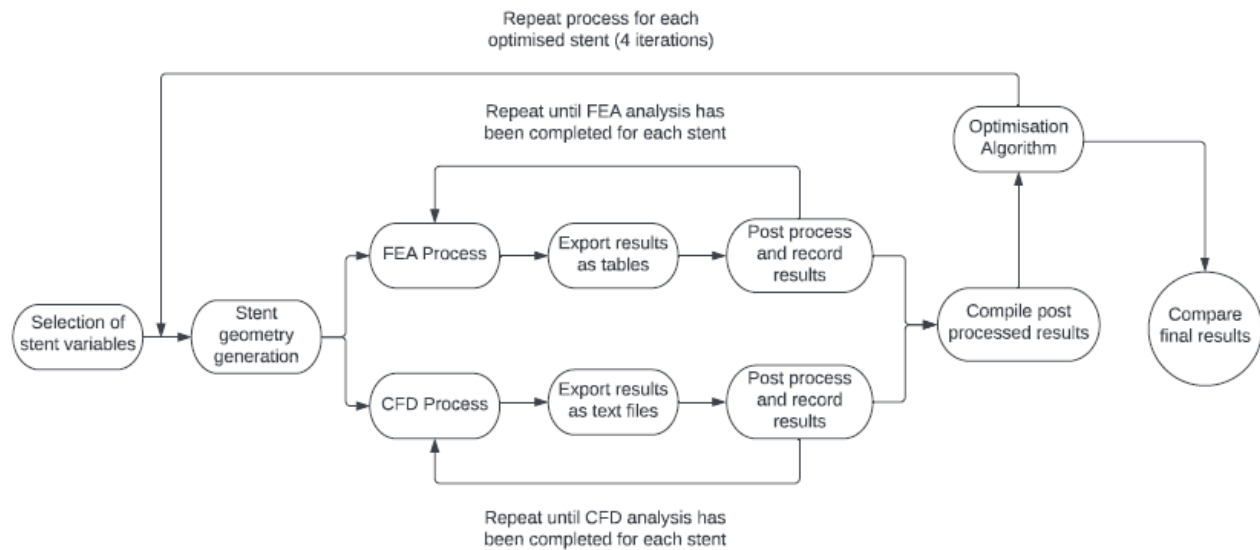


Figure 10 - Methodology flowchart

### 3.2. Stent Geometry

To effectively compare and contrast the performance of varying stent diameters, four differing sizes of stents were modelled. Specifically, 3mm, 3.2mm, 3.7mm and 4mm diameters were chosen. These were chosen due to their relevance and concurrent application in the commercial biomedical industry, as demonstrated in companies such as Boston Scientific and Medtronic who will primarily offer stent diameter ranges from 2.25mm to 4mm. Examples of their commercial stent properties are illustrated below in Figure 11 and Figure 12.

General Specifications	
Indications for Use	The Promus ELITE Everolimus-Eluting Platinum Chromium Coronary Stent System is indicated for improving luminal diameter in patients, including those with diabetes mellitus, with symptomatic heart disease or documented silent ischemia due to de novo lesions in native coronary arteries $\geq 2.25$ mm to $\leq 4.00$ mm in diameter in lesions $\leq 34$ mm in length.
Drug and Polymer	The drug-polymer coating consists of a PVDF-HFP polymer and the active pharmaceutical ingredient Everolimus.
Stent Material	Platinum Chromium (PtCr) Alloy
Available Stent Lengths	8, 12, 16, 20, 24, 28, 32, 38" (mm)
Available Stent Diameters	2.25", 2.50, 2.75, 3.00, 3.50, 4.00 (mm)

Figure 11 - Boston Scientific Promus ELITE general stent specifications **Error! Reference source not found.**

**Integrity RX Compliance**

Pressure (atm)	Stent Diameter Deployed Stent I.D. (mm)					
	2.25 <sup>†</sup>	2.50 <sup>†</sup>	2.75 <sup>†</sup>	3.00 <sup>†</sup>	3.50 <sup>†</sup>	4.00 <sup>†</sup>
6	2.15	2.40	2.65	2.85	3.25	3.70
7	2.20	2.45	2.70	2.90	3.30	3.75
8	2.20	2.50	2.75	2.95	3.40	3.85
9	2.25	2.55	2.80	3.05	3.45	3.90
10	2.30	2.55	2.85	3.10	3.50	4.00
11	2.35	2.60	2.90	3.10	3.55	4.05
12	2.35	2.65	2.90	3.15	3.60	4.10
13	2.40	2.65	2.95	3.20	3.65	4.15
14	2.45	2.70	3.00	3.25	3.65	4.20
15	2.50	2.75	3.05	3.30	3.70	4.25
16	2.50	2.80	3.10	3.30	3.75	4.30
17	2.55	2.80	3.15	3.35	3.80	4.35
18	2.60	2.85	3.20	3.40	3.85	4.40
19	2.65	2.90	3.25	3.45	3.90	4.45
20	2.75	2.95	3.30	3.50	3.90	—

Nominal pressure

Rated burst pressure\*

<sup>†</sup>Do not postdilate the 2.25–2.75-mm stents to greater than 3.50 mm.  
Do not postdilate the 3.00–4.00-mm stents to greater than 5.00 mm.

\*Rated burst pressure—do not exceed.

Figure 12 - Medtronic Integrity RX stent diameter pressure compliance [66]

19 unique stent geometries were generated for each diameter using SpaceClaim ANSYS 2019 R3. To assess their performances, tests examining the radial stiffness and wall shear stress of the stents were undertaken, due to their importance in determining overall stent durability, strength, and influence on adverse clinical outcomes. This was done using UNSW's VPN service, in which ANSYS 2019 R3 and its components could be accessed remotely using the Citrix Workspace app. Each unique stent was prescribed the stent parameters utilised previously in Deepan Kumar's work regarding stent diameters – derived similarly from Vanessa Luvio's Latin hypercube sampling data. By using an IronPython script written by Ramtin Gharleghi, these measures allowed for the convenient manipulation of stent parameters, and thus the creation of stents with differing characteristics including strut thickness and diameter, strut width, intra-strut angle, alignment type, cell height, connector type, and the number of connectors. However, due to technical difficulties in producing functional stent geometries for different diameters and lack of time, the inclusion of connectors in the stent design was omitted – resulting in a stent design containing only the struts. This was achieved by manually stripping out the relevant code in the IronPython script. Hence, the geometry essentially became a 'floating' stent design, in which the struts are not physically connected and hence may not provide the most accurate absolute values. Nonetheless, as all stent diameters are subject to the same design adjustment, a relative comparison of the stents will still serve sufficiently as a

representation of the different conditions to which the stents are subjected to. An example of a generated stent design is depicted below in Figure 13:

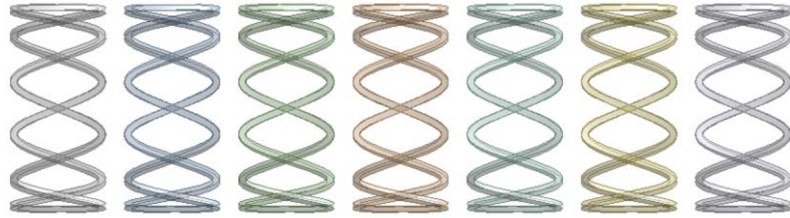


*Figure 13 - Stent ID 18, 1.5mm diameter*

### 3.3. Stent Materials

Several materials were considered for the application of the stent – to which four were chosen due to their favourable and relevant characteristics. These were the: L605 Cobalt Chromium (L605 CoCr), MP35N Cobalt Chromium (MP35N CoCr), Platinum Chromium (PtCr) and Stainless Steel (StSt). For simplicity, only the mechanical properties of each material were inputted into the engineering material database. The properties used are detailed below in Table 1:

*Table 1 - Mechanical properties of utilised materials*

Material	Properties					
	Density (kg/m <sup>3</sup> )	Young's Modulus (MPa)	Poisson's Ratio	Tensile Strength (MPa)	Yield Strength (MPa)	Ultimate Tensile Strength (MPa)
<b>L605 Cobalt Chromium</b>	9100	2.43e+05	0.29	500		1000
<b>MP35N Cobalt Chromium</b>	8442.4	2.01e+05	0.38	345		758
<b>Platinum Chromium</b>	7850	2.03e+05	0.285	480		834
<b>Stainless Steel</b>	7850	2.00e+05	0.3	250		460

L605 Cobalt Chromium was used to perform the bulk of the FEA analysis, and was used as the baseline material for the optimisation algorithm. After obtaining the final optimized stent designs, or ‘sopt4’ – each of the other listed materials were comparatively tested using the ‘sopt4’ parameters for every diameter.

### 3.4. FEA Set-up

#### 3.4.1. Geometry

Following the stent geometry generation process, the stent files were imported to a UNSW offered GUI based software, Katana OnDemand, which is a shared computational cluster located on campus. To begin the process, the respective stent geometry files were copied over to the Katana file database from myAccess, to which they are then imported into the static structural module. In measuring the radial strength of the stent, a static cylinder was generated about the diameter of the stent to simulate points of contact on its exterior surface. In creating the initial set-up, a few preliminary factors were first considered. Cross sectional strutted stents would require an additional cylinder of the same diameter to be generated, with the Boolean operation set to 'slice'. This was implemented to create an inner and outer partition of the stent contact area, effectively splitting the inner and outer faces. In the alternative case of a rectangular strutted cross section, this step was skipped as the external and internal faces are already separated into two different parts. Additionally, a plane was created for each stent cell, which was evenly spaced by the cell height along the stent length. This was performed to generate a vertical cut through the centre of each cell and can be seen in Figure 14 and Figure 15.

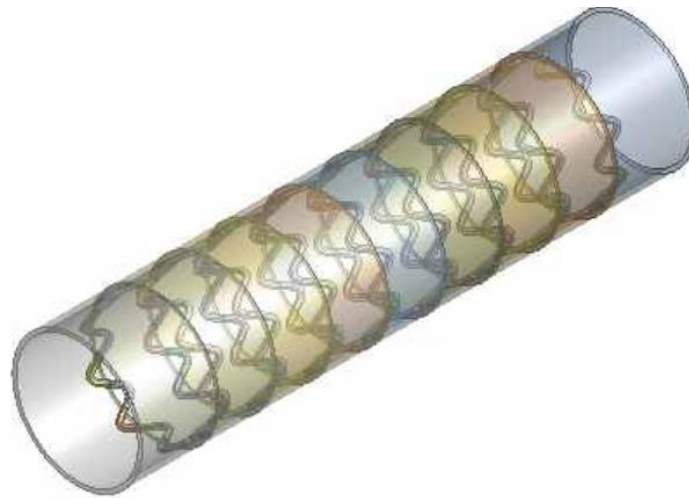
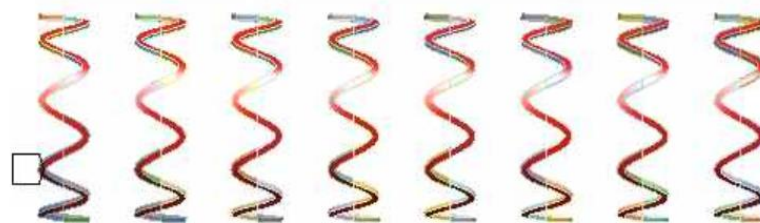


Figure 14 - FEA set-up geometry example

**Contact Region 157\_Target**  
 Contact Region 157\_Target



*Figure 15 - Simulated contact points of stent during FEA process*

### 3.4.2. Method

Following the completion of the geometrical procedures, the methodology of the FEA model set-up will be explored. The material of the stent was chosen as Cobalt Chromium L605 due to its superior properties in comparison to other commonly used materials, as explained previously in Section 2.5.3. The following procedures were taken in compliance to Vanessa Luvio's instructional brief [67]: the contact points of the stent were merged and promoted to a new named selection, creating two contact regions – 'Contact Region Contact' and 'Contact Region Target'. The cylinder was then suppressed, effectively leaving only the stent and 'Contact Region Target' to remain active, the latter of which encompasses the entire external contact region of the stent. A pressure load is subsequently generated by selecting the named selection as its parameter, simulating an inwards force of 0.02MPa. This was chosen due to previous research by Kumar et al. **Error! Reference source not found.**, where the applied pressure of 0.02MPa was likely to fall within the stent's elastic region.

From previously dividing the centre of each cell by inserting planes, this enabled the vertices of the cells to be selected as components for a displacement boundary condition. The axial and circumferential components of the stent are suppressed, allowing the radial component of the stent to be isolated in calculating the reaction forces in the radial direction, as shown below in Figure 16.

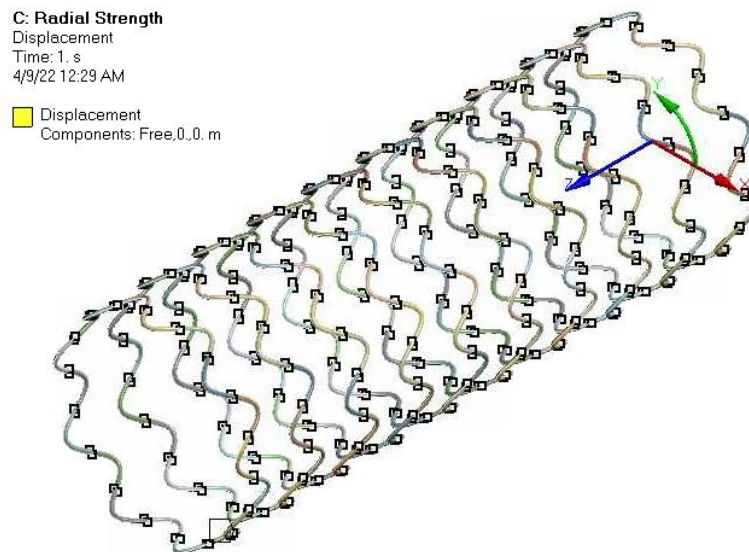


*Figure 16 - Displacement boundary condition for FEA set-up*

After applying the relevant boundary conditions, each individual stent geometry produced respective radial stiffness values, which were collected and compiled for the stent optimization process. Originally, bending and compression simulations were also conducted for the first few initial stress simulations, but due to lack of time and auxiliary nature of the data, only the radial simulations were performed.

### 3.5. CFD Set-up

To gauge the effect of blood flow on the differing stent diameters, the percentage of area with high wall shear stress (HWSS) and low wall shear stress (LWSS) was recorded and analysed. HWSS occurs when  $WSS \geq 2.5$  Pa, whilst LWSS occurs when  $WSS \leq 1$  Pa. This set-up was similarly conducted through the Katana OnDemand software, and utilised the same generated geometries. ANSYS CFX was used to simulate the desired data, and similar to the FEA process, a CFD simulation base-file supplied by Vanessa was used, which allowed for stent geometry files to be directly imported and implemented into the modules. Despite this, CFD simulation times still proved to be excessively high, and hence required an alternative, more efficient method. To combat this issue, a script written by Ramtin was utilized, which automated the meshing, solving, and post-processing components of the simulation, and resolved much of the time constraint problems faced. Another issue which was encountered during CFD generation was the inadequate disk space provided in the Katana database and thus required the deletion of the obtained CFD results after every four simulations.

To begin the process, the targeted stent geometry was imported into the simulation base-file. The pre-existing cylinder in the base-file was then resized to match the stent diameter of the imported geometry file. Subsequently, to produce an indentation of the stent in the cylinder, a function in ANSYS DesignModeler was used: the Boolean operation ‘subtract’, which allows for the stent material to be detracted from the contacting cylinder. The target body chosen would correspond to exclusively the cylinder, whilst the tool body chosen was exclusively the stent geometry. An example stent of this is shown below in Figure 17. After completing the initial geometrical procedures, Katana’s terminal function was used to initiate the CFD script – executed by running the command line ‘qsub setup.pbs’.

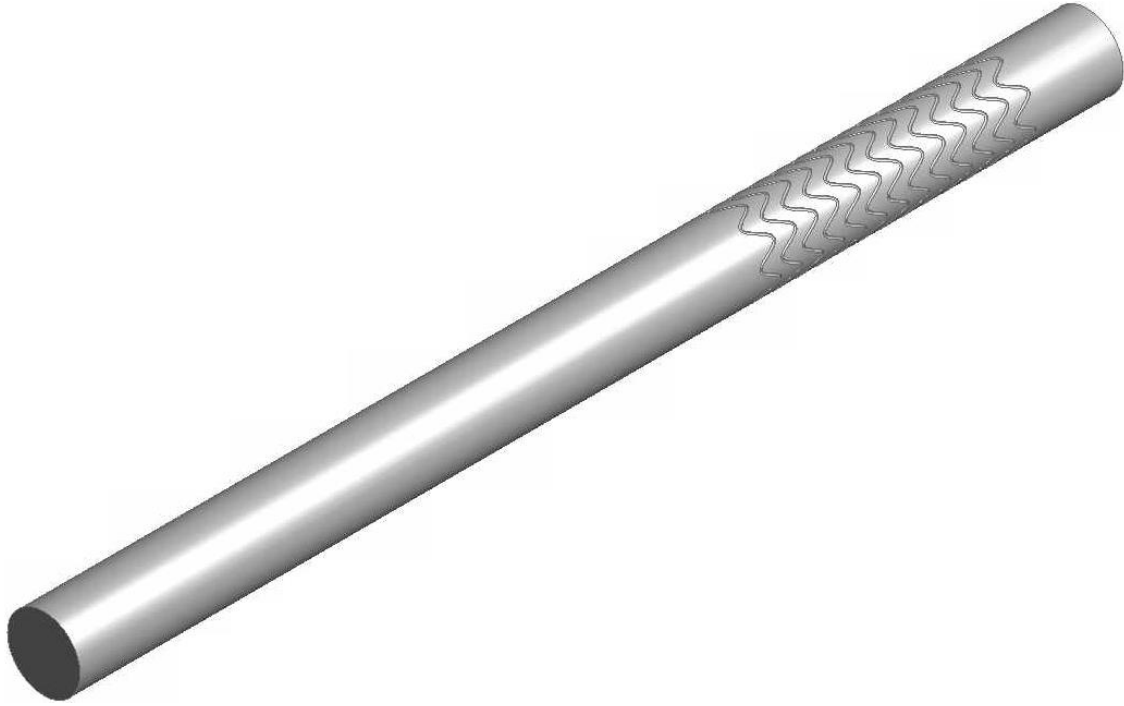


*Figure 17 - Stent cut-out operation on cylinder for CFD set-up*

### **3.6. Post-processing of results**

Following the FEA and CFD simulations, the results can be obtained in two respective forms. For FEA, by creating output parameters for the relevant results, such as cell height, total deformation, equivalent stress and contact region target surface area, these parameters are exported as an Excel file in a table format. An example of this is shown below in Figure 18. To determine the radial stiffness from these values, a series of quantitative formulas can be employed as shown below in Equation 1.

$$Radial\ stiffness = \frac{F}{\Delta D} \quad (1)$$

$$F = P \times A$$

Where:

$F$  = force

$\Delta D$  = total average directional deformation

$P$  = pressure

$A$  = surface area on outside of stent



```
#
# 03/09/2022 21:38:08
# The parameters defined in the project are:
#
# P1 - Active P3 - CellHe P4 - Mesh P5 - Force P12 - Mesl P13 - Forc P20 - Mesl P21 - Press P22 - Total P23 - Total P24 - Total P25 - Equiv P26 - Equiv P27 - Equiv P28 - Mesl P29 - Mesl P30 - Mesl P31 - Contact Region 109_Target Surface Area [m^2]
#
# The following header line defines the name of the columns by reference to the parameters.
Name P1 P3 P4 P5 P12 P13 P20 P21 P22 P23 P24 P25 P26 P27 P28 P29 P30 P31
DP 0 10.976 1.557 0.032 -0.01 0.032 0.004 0.032 0.02 0.000203 0.000232 0.000162 2.851102 110.5684 0.05195 280252 1.07E-05
DP 1 10.976 1.557 0.032 -0.005 0.032 0.002 0.032 0.01
DP 2 10.976 1.557 0.032 -0.001 0.032 0.001 0.032 0.005
```

Figure 18 - Exported Excel data for FEA post-processing

This process is repeated for all 19 unique stent designs, of which the formula utilising Equation 1 is embedded within the radial stiffness column in the Microsoft Excel file. This is shown below in Figure 19.

Stent #	DP #	P1 - ActiveLength (Bending) [mm]	P3 - CellHeight (Radial) [mm]	P4 - Mesh Size (Bending) [mm]	P5 - Force X Component (Bending) [N]	P12 - Mesh Size (Compression) [mm]	P13 - Force Z Component (Compression) [N]	P20 - Mesh Size (Radial) [mm]	P21 - Pressure Magnitude (Radial) [MPa]	P22 - Total Deformation Average (R) [mm]	P23 - Total Deformation Maximum (R) [mm]	P24 - Total Deformation Minimum (R) [mm]	P25 - Equivalent Stress Average (R) [MPa]	P26 - Equivalent Stress Maximum (R) [MPa]	P27 - Equivalent Stress Minimum (R) [MPa]	P28 - Contact Region 97_Target Surface Area [m^2]	P28 - Contact Region 97_Target Surface Area [m^2]	Radial Stiffness (N/m)
0	DP 0	10.976	1.08	0.032	-0.01	0.032	0.004	0.032	0.02	0.001188	0.002639	0.000453	6.139084	571.7223	0.029159	1.53E-05	1.53E+01	1.29E-04
2	DP 0	10.976	1.435	0.032	-0.01	0.032	0.004	0.032	0.02	0.001866	0.006632	0.000165	6.498062	418.5429	0.027537	1.78E-05	1.78E+01	9.55E-05
3	DP 0	10.976	1.557	0.032	-0.01	0.032	0.004	0.032	0.02	0.000266	0.000301	0.000214	3.220568	142.4496	0.063249	1.16E-05	1.16E+01	4.35E-04
4	DP 0	10.976	1.8	0.032	-0.01	0.032	0.004	0.032	0.02	0.000313	0.000359	0.000256	3.594741	159.9817	0.093989	9.96E-06	9.96E+00	3.18E-04
12	DP 0	10.976	1.477	0.032	-0.01	0.032	0.004	0.032	0.02	0.000426	0.000502	0.000322	4.750566	218.4805	0.104444	1.09E-05	1.09E+01	2.56E-04
17	DP 0	10.976	1.358	0.032	-0.01	0.032	0.004	0.032	0.02	5.17E-05	0.0001	1.65E-05	0.680399	51.37576	0.00802	2.43E-06	2.43E+00	4.70E-04
18	DP 0	10.976	1.702	0.032	-0.01	0.032	0.004	0.032	0.02	0.000784	0.000958	0.000556	4.780998	359.5678	0.028898	1.82E-05	1.82E+01	2.32E-04
19	DP 0	10.976	1.003	0.032	-0.01	0.032	0.004	0.032	0.02	5.37E-05	0.000138	3.70E-05	1.356193	114.0327	0.007286	1.58E-05	1.58E+01	2.94E-03
26	DP 0	10.976	1.677	0.032	-0.01	0.032	0.004	0.032	0.02	0.000301	0.000334	0.000254	2.506357	218.0477	0.014794	1.97E-05	1.97E+01	6.52E-04
31	DP 0	10.976	1.778	0.032	-0.01	0.032	0.004	0.032	0.02	0.000814	0.000932	0.000736	6.127232	277.4344	0.049759	1.97E-05	1.97E+01	2.42E-04
32	DP 0	10.976	1.285	0.032	-0.01	0.032	0.004	0.032	0.02	0.00105	0.001286	0.00088	5.201726	481.5693	0.02746	3.47E-05	3.47E+01	3.31E-04
38	DP 0	10.976	0.87	0.032	-0.01	0.032	0.004	0.032	0.02	0.000823	0.001474	1.99E-05	5.438735	332.2475	0.017632	3.96E-05	3.96E+01	4.81E-04
44	DP 0	10.976	1.18	0.032	-0.01	0.032	0.004	0.032	0.02	0.000243	0.00033	1.96E-06	3.880113	123.325	0.049764	2.14E-05	2.14E+01	8.80E-04
45	DP 0	10.976	1.681	0.032	-0.01	0.032	0.004	0.032	0.02	0.000239	0.000259	0.000225	2.666826	162.4701	0.024491	2.57E-05	2.57E+01	1.07E-03
48	DP 0	10.976	1.383	0.032	-0.01	0.032	0.004	0.032	0.02	0.00041	0.000461	0.000374	3.098317	272.8875	0.011321	3.46E-05	3.46E+01	8.43E-04
49	DP 0	10.976	1.883	0.032	-0.01	0.032	0.004	0.032	0.02	0.000421	0.000652	1.87E-06	3.844187	200.7137	0.017353	2.11E-05	2.11E+01	5.00E-04
52	DP 0	10.976	1.467	0.032	-0.01	0.032	0.004	0.032	0.02	0.000352	0.000479	4.69E-06	5.346311	157.565	0.050096	1.51E-05	1.51E+01	4.29E-04
53	DP 0	10.976	1.508	0.032	-0.01	0.032	0.004	0.032	0.02	0.001249	0.001587	0.001014	5.718241	472.1721	0.139483	2.99E-05	2.99E+01	2.39E-04
59	DP 0	10.976	1.743	0.032	-0.01	0.032	0.004	0.032	0.02	0.000705	0.000807	0.000639	4.010668	413.9776	0.006938	2.90E-05	2.90E+01	4.11E-04
opt1	DP 0	10.976	0.981	0.032	-0.01	0.032	0.004	0.032	0.02	0.00052	0.000579	0.00043	3.891063	288.3737	0.037101	1.79E-05	1.79E+01	3.43E-04
opt2	DP 0	10.976	1.09	0.032	-0.01	0.032	0.004	0.032	0.02	0.000491	0.000554	0.000413	3.895245	272.1622	0.04342	1.65E-05	1.65E+01	3.35E-04
opt3	DP 0	10.976	0.99	0.032	-0.01	0.032	0.004	0.032	0.02	0.000484	0.000529	0.000428	3.844512	238.8343	0.044854	1.49E-05	1.49E+01	3.08E-04
opt4	DP 0	10.976	1.07	0.032	-0.01	0.032	0.004	0.032	0.02	0.000477	0.000525	0.000411	3.743905	252.3804	0.038729	1.55E-05	1.55E+01	3.25E-04

Figure 19 - Compilation of post-processing results for FEA

For CFD, a viewable text file named 'report.txt' is outputted at the conclusion of the CFD simulation, and contains the percentage area of the LWSS and the HWSS. In particular, the adverse range of WSS (WSS  $\leq 1$  Pa and WSS  $\geq 2.5$  Pa) is targeted to be minimized, whilst the radial stiffness values are optimal at greater values. An example visual representation of the flow (from CFD-Pre) actioned upon the stent is shown below in Figure 20:

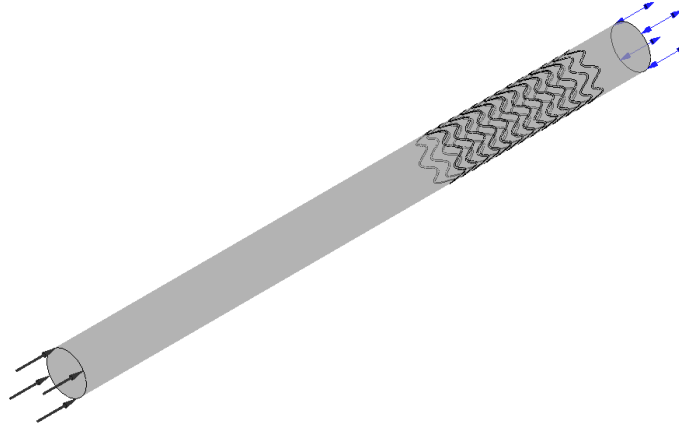


Figure 20 - CFX-Pre conditions for 'sopt1\_1.5mm' stent

### 3.7. Optimisation algorithm

The multi-objective optimisation process was developed to optimise specific properties of the stent: its radial stiffness, while minimizing the low time averaged wall shear stress (LTWASS) and HWSS. The algorithm operates by analysing the inputs of the stent geometry and post-processed FEA and CFD results and after execution, the script will ultimately generate a new recommended array of stent parameters. To achieve a sufficient number of stent designs required for the optimization algorithm, the post processed parameters of 19 unique stent designs were inputted into the 'Data\_2' Excel directory. This file acts as the primary matrix dataset that the optimisation algorithm 'Algorithm\_2.m' uses as a function within its script. As shown below in Figure 21, an example output is produced by the algorithm, depicting the new recommended stent parameters.

```
ans =  
1.0000  72.0711  113.3904  38.5722      0  1.7061  2.0000  4.0000  9.0000
```

Figure 21 - Example output produced by one iteration of the optimisation algorithm

This optimisation process is repeated four times to achieve a convergence of stent parameters. Hence, new stent geometry designs were generated using the obtained optimised stent parameters, which were imported into the FEA and CFD procedures. This iterative process can be visualised using the flowchart depicted earlier in Figure 10. Hence, a snapshot of the complete results were compiled into a separate Excel file for convenience and accessibility, shown below in Table 2.

Table 2 - Compiled optimised results table for 3mm stent

3mm							
Stent ID	CS	SD1 ( $\mu\text{m}$ )	SD2 ( $\mu\text{m}$ )	SA ( $^{\circ}$ )	AT ( $^{\circ}$ )	CH (mm)	NP
0	1	103.43	73.53	43.56	0	1.080	7
2	1	76.38	106.45	38.59	0	1.435	9
3	1	85.01	82.21	47.69	180	1.557	9
4	1	73.67	78.94	46.20	0	1.800	6
12	1	66.87	74.31	45.11	180	1.477	6
17	1	119.47	62.86	44.98	180	1.358	9
18	1	83.07	101.93	30.52	0	1.702	6
19	1	108.92	65.44	34.95	180	1.003	9
26	1	116.37	117.69	33.12	0	1.677	8
31	2	71.65	Inf	31.55	180	1.778	8
32	2	98.38	Inf	27.57	0	1.285	6
38	2	78.34	Inf	32.32	0	0.870	7
44	2	72.35	Inf	46.02	0	1.180	9
45	2	108.33	Inf	37.44	180	1.681	9
49	2	87.98	Inf	33.15	180	1.883	9
52	2	63.39	Inf	45.72	0	1.467	9
53	2	91.96	Inf	26.09	0	1.508	6
59	2	106.04	Inf	26.70	0	1.743	8
48	2	116.06	Inf	33.55	0	1.383	7
sopt1	2	93.80	Inf	39.55	0	0.874	7
sopt2	2	65.70	Inf	27.77	0	0.830	7
sopt3	2	64.08	Inf	31.97	0	1.014	7
sopt4	2	75.54	Inf	28.74	0	0.934	7

## 4. Results and discussion

### 4.1. Multi-objective Optimisation

In generating the optimised stent designs, initial sampling of 19 unique stent geometries was conducted. The data obtained for the responsible stent diameters are shown below in Table 3. This data consists of the HWSS, LWSS and radial stiffness values.

*Table 3 – Initial results table for stent diameters*

	RESULTS (3MM)			RESULTS (3.2MM)			RESULTS (3.7MM)			RESULTS (4MM)		
STENT ID	HWSS (%) Area)	LWSS (%) Area)	Radial Stiffness (N/mm)	HWSS (%) Area)	LWSS (%) Area)	Radial Stiffness (N/mm)	HWSS (%) Area)	LWSS (%) Area)	Radial Stiffness (N/mm)	HWSS (%) Area)	LWSS (%) Area)	Radial Stiffness (N/mm)
0	48.00	9.45	244.52	8.00	11.56	224.21	1.40	24.98	224.21	0.00	92.74	129.15
2	72.30	4.86	518.21	8.60	5.95	399.37	8.60	6.00	110.32	0.00	96.90	95.50
3	70.10	5.79	268.09	5.90	7.04	747.01	0.30	14.97	528.24	0.00	94.70	435.03
4	78.70	4.43	168.61	5.20	5.29	517.19	0.10	11.45	357.43	0.00	96.11	318.06
12	76.00	4.62	135.15	5.60	5.54	451.32	0.00	12.19	315.04	0.00	96.09	256.05
17	53.20	8.96	942.03	5.90	10.80	805.60	1.80	22.70	565.73	0.00	94.78	469.97
18	72.10	5.67	457.02	9.30	6.82	384.31	0.10	15.29	276.74	0.00	95.66	231.90
19	51.70	12.37	827.19	9.50	14.68	712.35	1.70	27.55	1014.33	0.00	94.71	2942.98
26	59.80	7.49	1306.17	10.00	9.15	1120.34	1.30	20.31	794.97	0.00	93.81	652.08
31	81.20	2.35	493.56	5.10	3.09	404.91	0.80	9.00	290.87	0.00	96.17	241.65
32	62.80	4.47	756.19	9.90	5.80	623.62	1.20	15.16	394.84	0.00	93.43	330.96
38	11.90	4.60	933.63	9.80	6.04	859.36	1.30	18.92	567.20	0.00	92.83	480.87
44	76.40	3.18	1784.66	5.20	4.09	1398.60	2.00	11.55	1105.12	0.00	96.00	879.52

<b>45</b>	73.60	3.56	2385.65	6.60	4.54	1790.37	2.40	12.59	1314.73	0.00	94.99	1074.34
<b>48</b>	66.30	4.51	929.86	8.70	5.73	1446.32	2.20	16.01	542.16	0.00	93.41	500.43
<b>49</b>	81.00	2.45	979.05	5.20	3.22	714.98	1.20	9.14	551.26	0.00	96.12	428.84
<b>52</b>	83.30	2.04	464.80	3.70	2.67	889.75	1.10	7.58	290.76	0.00	97.18	239.33
<b>53</b>	73.45	3.20	906.28	9.00	3.40	397.17	0.90	12.39	565.27	0.00	94.28	410.96
<b>59</b>	70.40	3.93	1785.66	8.80	5.04	772.99	1.20	14.50	1033.48	0.00	94.35	842.78

The results were then updated using the optimisation algorithm, which outputted: 14 non-dominated (ND) solutions for the ‘3mm’ stent, 6 ND solutions for the ‘3.2mm’ stent, 8 ND solutions for the ‘3.7mm’ stent, and 8 ND solutions for the ‘4mm’ stent. This is shown below in Figures Figure 22, Figure 23, Figure 24 and Figure 25. For reference, a non-dominated solution is defined as a solution that has at least one objective value that is better than another stent design [67].

Three objectives are contrasted against one another in these figures: Objective 1 is a measure of minimizing HWSS, Objective 2 a measure of minimizing low TAWSS and Objective 3 a measure of maximizing radial stiffness.

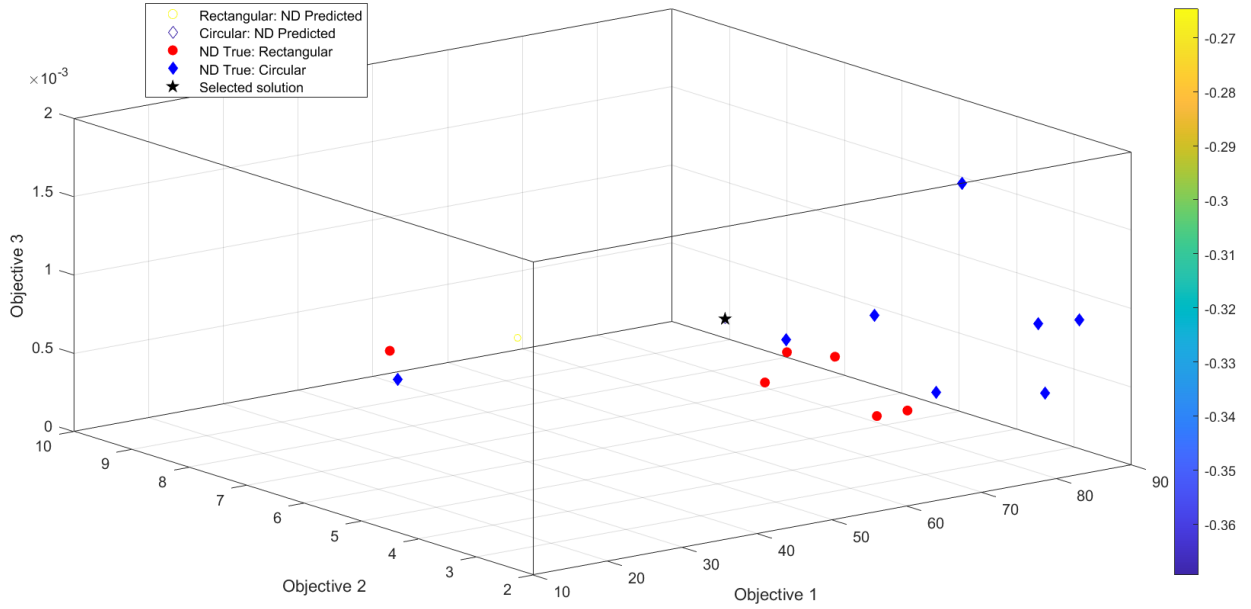


Figure 22 - Comparison of objectives for '3mm' diameter stent for the non-dominated solutions

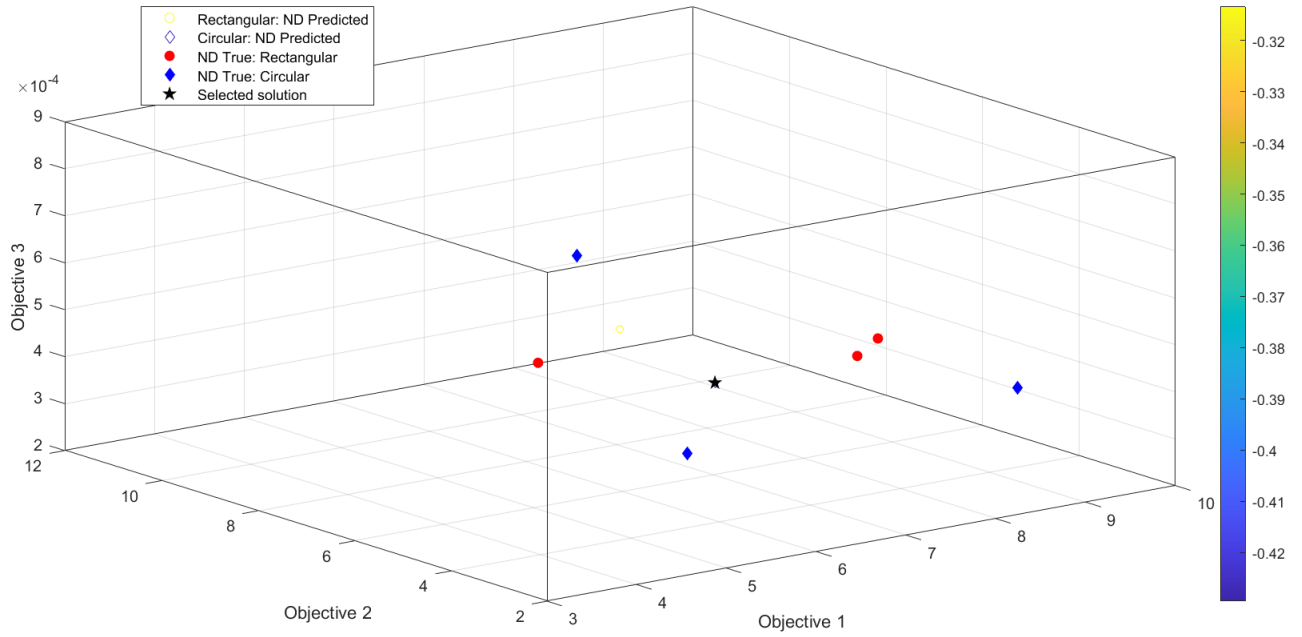


Figure 23 - Comparison of objectives for '3.2mm' diameter stent for the non-dominated solutions

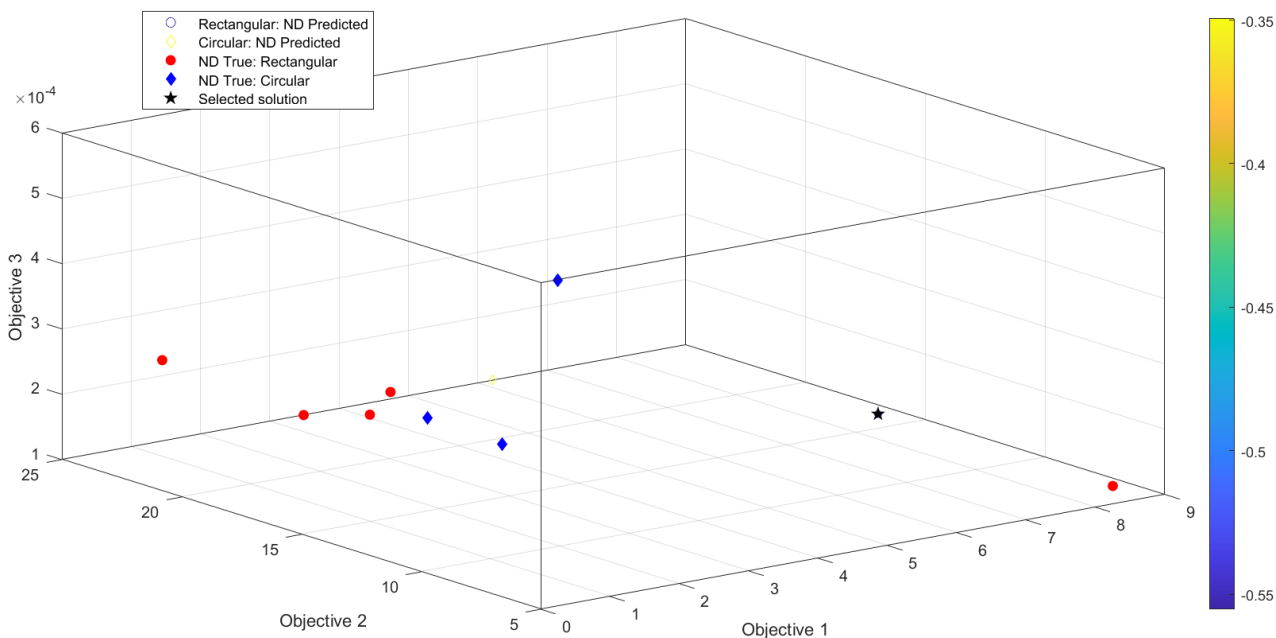


Figure 24 - Comparison of objectives for '3.7mm' diameter stent for the non-dominated solutions

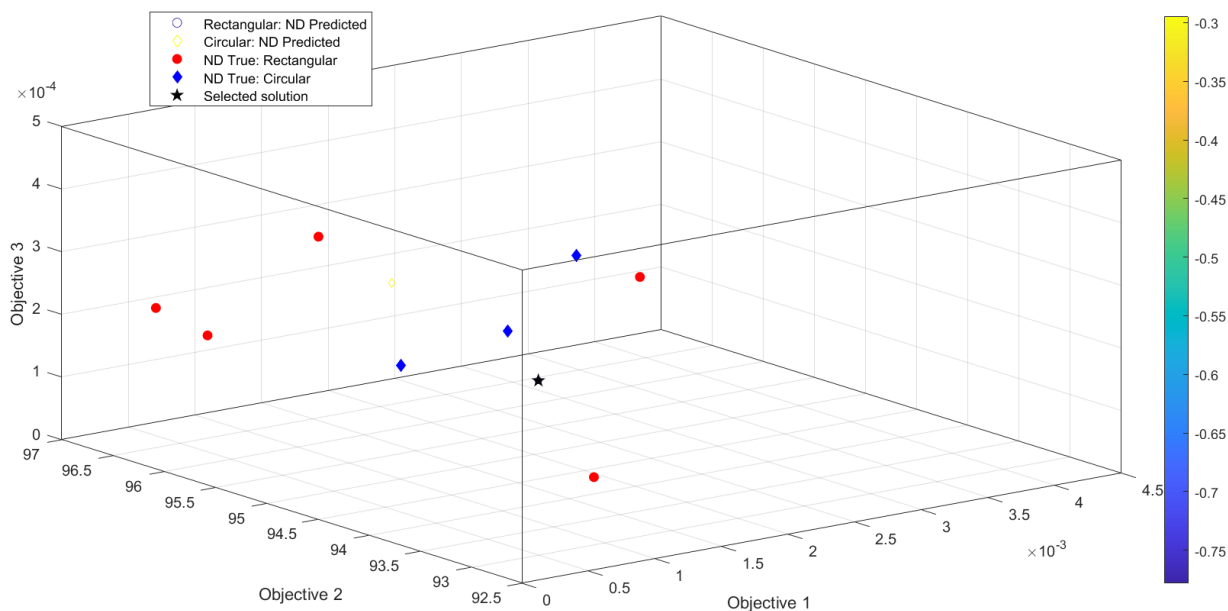


Figure 25 - Comparison of objectives for '4mm' diameter stent for the non-dominated solutions

In executing the optimisation algorithm script, as described in the methodology section 3.7, a new recommended updated stent design is then selected and iteratively recycled to the 'Data\_2' matrix to contribute towards another stent design. This was performed four times for each stent diameter, to which their designs are shown below in Figure 26.

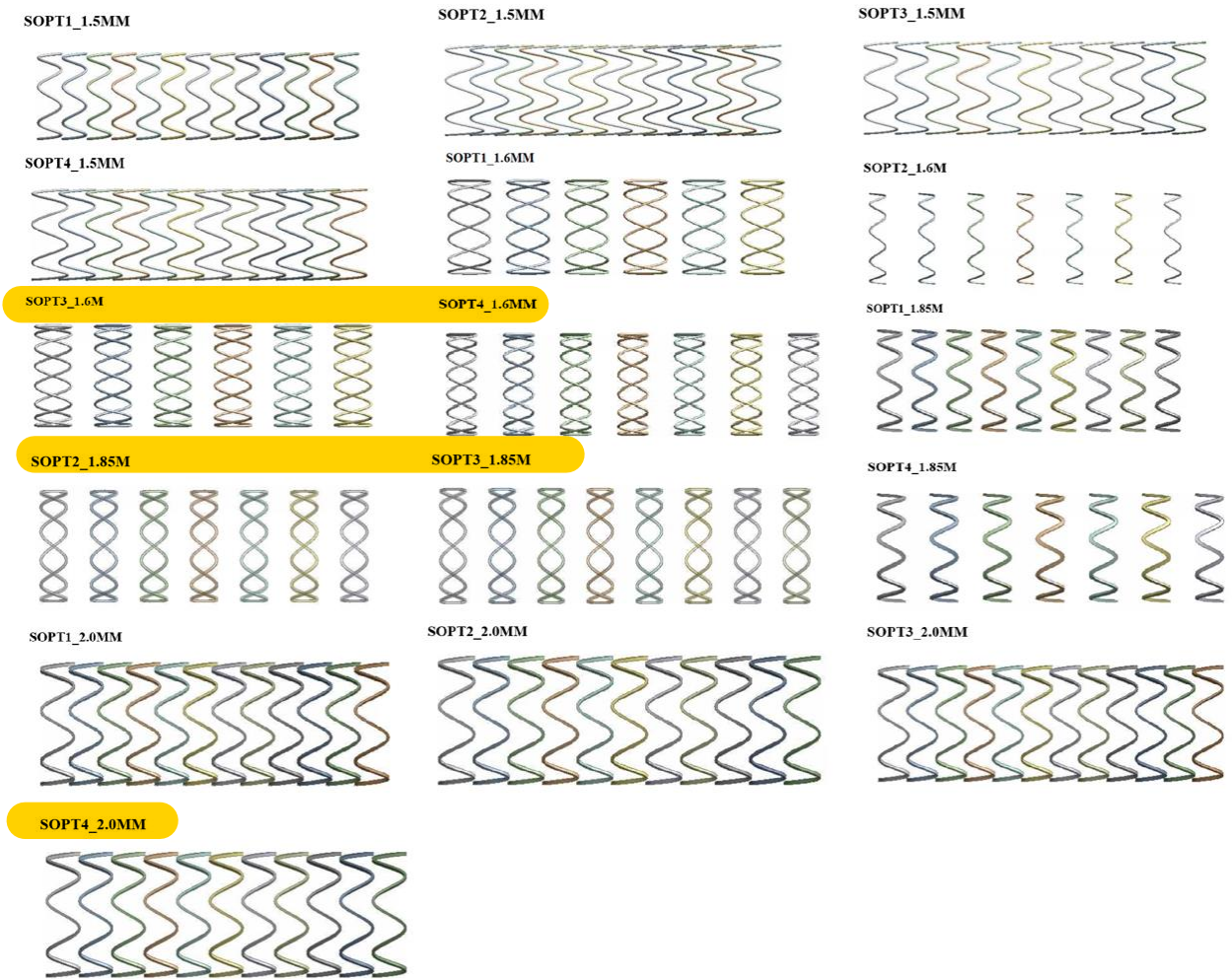


Figure 26 - Compilation of optimised stent design variations

From inspecting the stent geometries obtained – the alignment types of the 3mm and 4mm diameter stents remained at 0°, whilst the 3.2mm and 3.7mm were more erratic in their adjusted stent designs. The design parameters of the 4mm diameter stents were also notably similar throughout each optimisation iteration, in which its alignment, peaks, and cell height remained very close in value to one another.



Listed below in Table 4 are the updated, optimized stent designs for stent diameters: ‘3mm’, ‘3.2mm’, ‘3.4mm’ and ‘4mm’, with ‘sopt4’ as the final design iteration. It was noted that for increasing diameter sizes, rectangular stents were more heavily favoured, whilst smaller stent diameters favoured circular cross sections. The radial stiffness values were shown to vary amongst stent values, with the 3mm stent exhibiting the highest average radial stiffness value. However, if the outlier of ‘sopt1’ is removed, the 3.7mm stent exhibited the highest average radial stiffness value, while the 4mm stent exhibited the lowest.

*Table 4 - Complete optimised results table for all stent diameters*

<b>3MM</b>										
<b>STENT PARAMETERS</b>								<b>RESULTS</b>		
<b>Stent ID</b>	<b>CS</b>	<b>SD1 (<math>\mu</math>m)</b>	<b>SD2 (<math>\mu</math>m)</b>	<b>SA (°)</b>	<b>AT (°)</b>	<b>CH (mm)</b>	<b>NP</b>	<b>HWSS (%) Area)</b>	<b>LWSS (%) Area)</b>	<b>Radial Stiffness (N/mm)</b>
<b>sopt1</b>	2	93.80	Inf	39.55	0	0.874	7	51.4	5.45	2106.36
<b>sopt2</b>	2	65.70	Inf	27.77	0	0.830	7	59.8	3.64	460.94
<b>sopt3</b>	2	64.08	Inf	31.97	0	1.014	7	72.6	2.88	425.66
<b>sopt4</b>	2	75.54	Inf	28.74	0	0.934	7	59.9	4.28	770.48
<b>3.2MM</b>										
<b>sopt1</b>	2	80.17	Inf	31.85	180	1.8789	8	4.9	3.01	294.53
<b>sopt2</b>	2	65.72	Inf	46.24	0	1.683	9	3.3	2.44	697.64
<b>sopt3</b>	2	80.93	Inf	29.15	180	1.864	8	5.4	3.07	387.22

R.Lu – Multi-Objective Optimisation of Stent Designs Focussing on Vessel Calibre

<b>sopt4</b>	2	80.78	Inf	33.71	180	1.826	8	5.4	3.36	587.28
<b>3.7MM</b>										
<b>sopt1</b>	1	74.00	95.82	36.52	0	1.324	9	0.9	15.90	714.73
<b>sopt2</b>	1	70.49	74.23	48.16	180	1.691	6	0.1	10.87	331.25
<b>sopt3</b>	1	69.66	65.74	49.96	180	1.597	6	0.0	11.54	342.83
<b>sopt4</b>	1	72.07	113.39	38.57	0	1.706	9	0.7	11.66	888.12
<b>4MM</b>										
<b>sopt1</b>	1	103.14	71.08	38.53	0	0.981	7	0.0	91.50	343.44
<b>sopt2</b>	1	97.13	72.52	39.19	0	1.090	7	0.0	92.16	335.45
<b>sopt3</b>	1	102.63	62.50	41.05	0	0.990	7	0.0	92.79	308.03
<b>sopt4</b>	1	106.18	69.51	40.10	0	1.070	7	0.0	92.55	324.74

## 4.2. FEA Results

The radial stiffness values obtained for each unique stent were compiled and averaged out to form the graph shown below in Figure 27. The values used here account for all the values obtained for the primary stent material of L605 Cobalt Chromium, including the optimized stent results. As can be observed from the graph, a decreasing linear trend in radial stiffness performance is seen with the increase of stent diameter – approximating about a 38.8% decrease in average value.

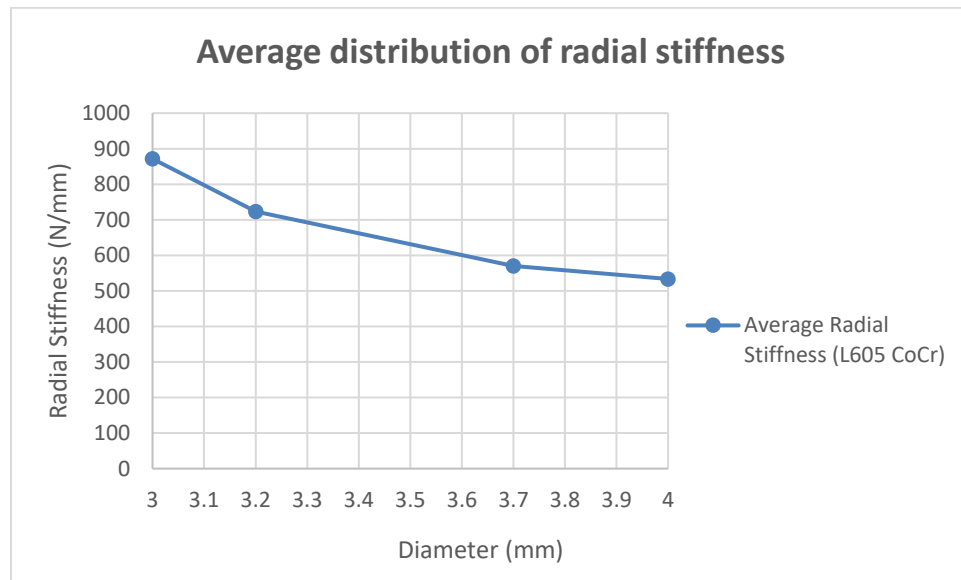


*Figure 27 - Average radial stiffness distribution among stent diameters*

For the MP35N CoCr, PtCr and StSt materials, their performance based off of the final optimized stent design of 'sopt4' was recorded. As such, the contrast between these materials and corresponding diameters are illustrated below in Figure 28. A tabulated view of the raw data utilised is found in Table 4. In Figure 28, a clear decreasing linear trend can be seen for each stent material – with the recommended L605 Cobalt Chromium material consistently outperforming other stent materials. As the stent diameter was increased from '3mm' to '3.2mm', radial stiffness performance slightly dropped for all material types. However, it was also noted that for MP35N Cobalt Chromium, Platinum Chromium and Stainless Steel, the linearly decreasing curve was flattened, and that the three material types achieved very similar radial stiffness values – in contrast to their '3mm' performance. The stent designs performed best using the '3.7mm' design, and worst with the '4mm' design, with the '3.7mm' L605 CoCr material almost tripling the radial stiffness value of the '4mm' L605 CoCr material.

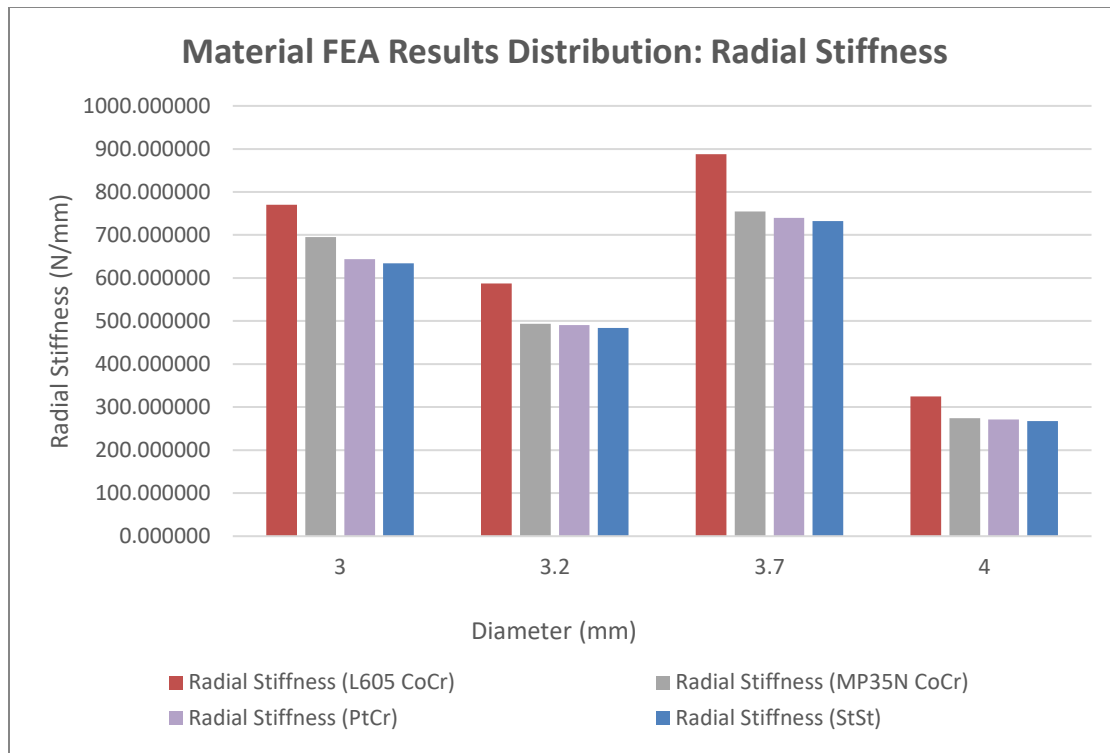


Figure 28 - Radial stiffness values of varying stent diameters and their material

Additionally, visual demonstrations of the resultant radial compression were supplied by the static structural module of ANSYS, autoscaled from true deformation. For reference, Figure 30 depicts the final optimised stents of each diameter and material. From examining the total deformation values obtained, the overall deformation imposed on the stents were relatively low – deflecting in the range of 1-9 micrometers. Concentration of stress was found to be focused towards the strut edges, or its peaks and troughs. Conversely, deformation was minimal towards the midpoint, or centres of the stent struts. Some discrepancies were noted in some of the designs, however, where some of the stent struts would deform irregularly. This may be attributed to the lack of connectors which would have provided a more stable structure and mechanical integrity. Furthermore, due to lack of resolution, the stents designs appear black in colour. As such, a close up view of one of the stents is provided below in Figure 29.

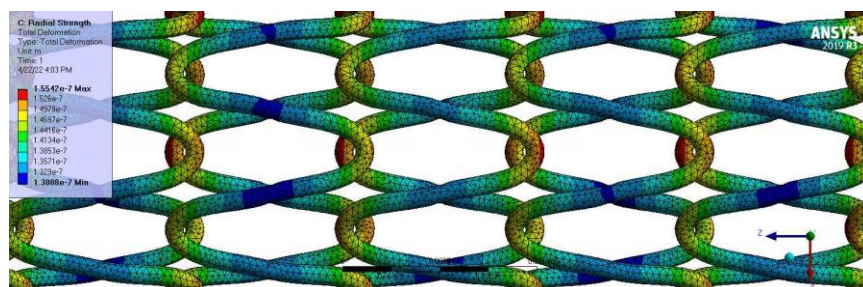


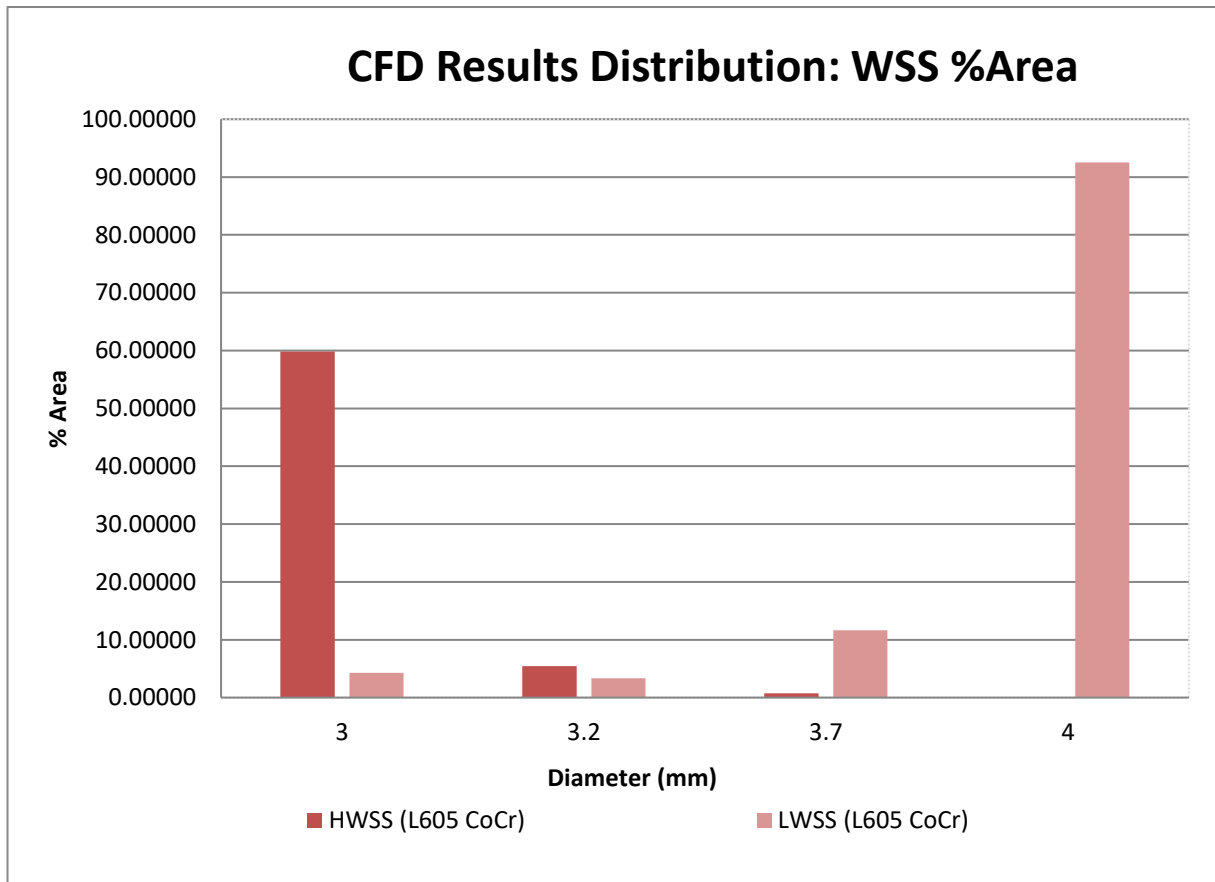
Figure 29 - Close-up view of 'Sopt1\_1.5mm'



Figure 30 - Optimised stent deformation geometry and value

### 4.3. CFD Results

The obtained WSS and LWSS percentage area values are illustrated below in Figure 31. A tabulated view of the raw data utilised can be found in the appropriate columns in Table 4. From examining Figure 31, the percentage of area with HWSS values heavily decreased for increasing stent diameters, but was also found to be inversely proportional to the percentage of area with LWSS values. This is demonstrated as seen in the 3mm diameter increase to the 3.2mm diameter, which the percentage of HWSS area rapidly decreased, while the percentage of LWSS area similarly slightly decreased. However, for the 3.7mm and 4mm diameter stents, the percentage of LWSS area began to increase, peaking in the range of 90-100 for the 4mm stent.



*Figure 31 - HWSS and LWSS %Area values of varying stent diameters and their materials*

Visual interpretations of the LTAWSS distribution were recorded from accessing the CFD-post simulations, and is shown below in Figure 32. Notably, areas of LWTASS were particularly concentrated in the peaks and troughs among the stent designs –growing more severe as stent diameters were increased.



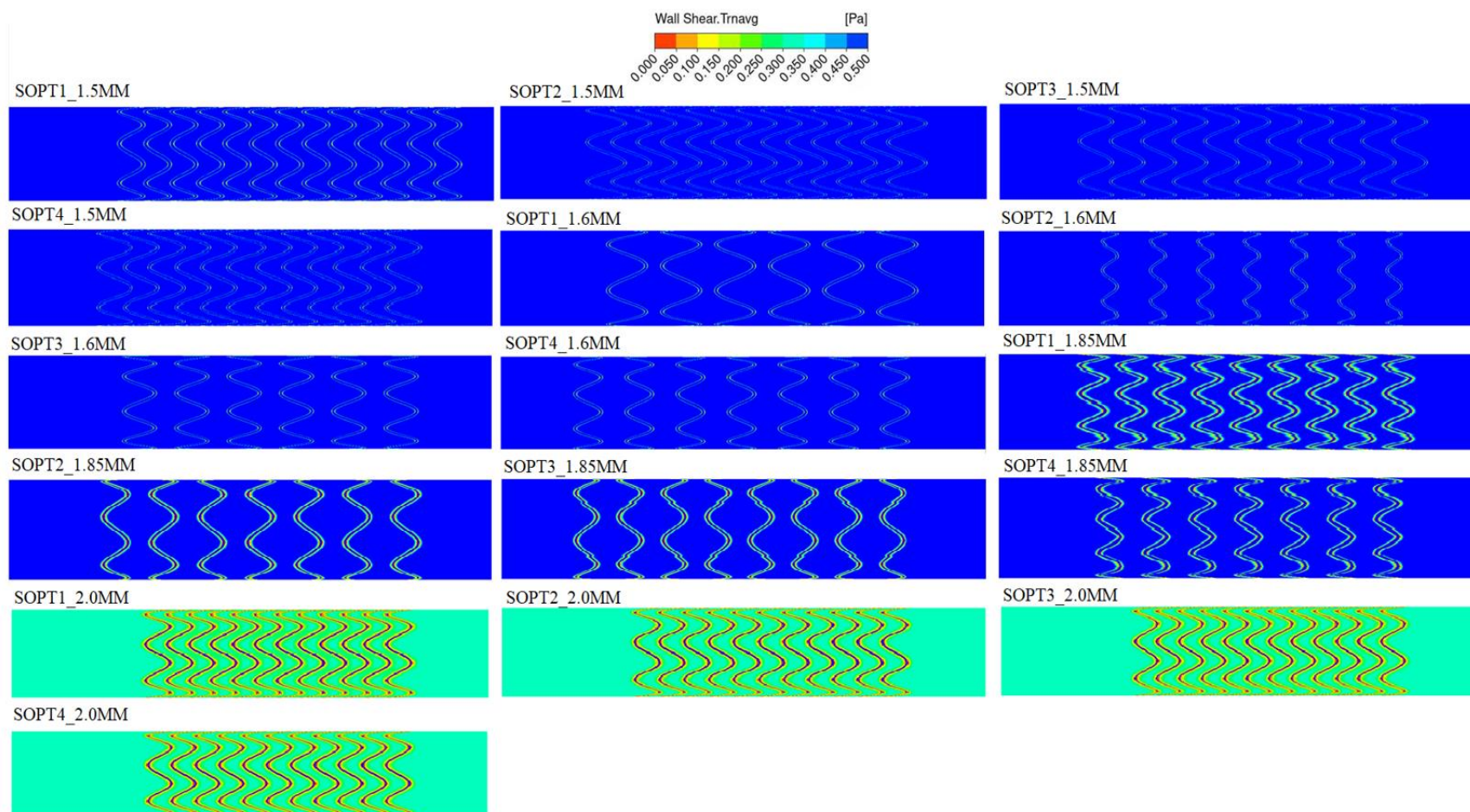


Figure 32 – Time-averaged wall shear stress distribution along optimised stent geometry

#### 4.4. Discussion

By varying the diameter of stent geometries, significant impacts were exhibited on the mechanical strength of stents and the percentage of area affected by WSS values. From examining Figure 27, it was suggested that: the lower the diameter of the stent, the stiffer the stent composition. This is consistent with a stent crimping process in a publication written by Zhao et al. [69], where smaller stent sizes produced increasingly larger strengths. This is further supported by contemporary research which has suggested the tenet that ‘smaller is stronger’ due to a process known as mechanical annealing. The percentage of area of WSS was also observed to follow an ‘inverse normal’ distribution curve, in which HWSS areas were much more prominent in smaller stent diameters, whilst LWSS areas dominated the larger stent diameters. Despite the exclusion of connectors, successful trends were observed in the compilation of results, and allowed for valuable insights pertaining to the radial stiffness and WSS of different stent diameters and materials to be obtained.

The FEA simulations were split into two sections. The first graph, Figure 27, depicted the average radial stiffness values recorded for all stent geometries with the L605 CoCr material. The second graph, Figure 28, depicted the distribution of values obtained from varying stent materials using the final ‘sopt4’ stent design parameters. From a non-contextual standpoint, the results obtained in Figure 27 alluded towards the superiority of smaller stent diameters due to their higher radial stiffnesses. However, adverse clinical outcomes such as intimal hyperplasia are not accounted for in this study. Despite their high radial stiffnesses, the margin for error for lower stent diameters becomes much lower, where even the small amounts of intimal growth may induce ISR. Hence, this data should only be adopted for quantitative purposes, as any conclusions drawn without this consideration may cause misinterpretations. In inspecting the second graph, the impact of different materials types were examined. In particular, material density would linearly decrease with radial stiffness values – which was evident in the L605 CoCr material achieving the greatest mechanical performance. As such, to confirm this hypothesis, additional materials which exhibit greater densities should be tested for their resultant radial stiffness values. A distribution incorporating all 19 unique stent geometries for each material would be ideal for accuracy, but was excluded due to lack of time. For future reference, inclusion of these data points would be substantially beneficial in providing additional results.

Conversely, the CFD results exhibited a much more consistent variation as stent diameters were increased. Lower stent diameters had a much higher proportion of LWSS area relative to HWSS area, but were observed to be generally inversely correlated with one another. This is also consistent with current literature



[70], to which the overexpansion of stents were shown to markedly increase the area of the vessel subjected to low WSS. This is also observed in Figure 32, of which LWSS areas gradually increase for each larger stent diameter, primarily at the peaks and troughs. However, in current common practices, smaller stent diameters have been associated with greater adverse clinical outcomes, and as Figure 31 demonstrates – provides the greatest area of HWSS. By following this advice, this data may suggest that HWSS may be a greater contributor to adverse clinical outcomes than previously believed. Nonetheless, the high percentage of LWSS area in the ‘4mm’ stent diameter is a concerning figure, and may discourage the contemporary application of stent overexpansion.

In both the optimal FEA and CFD models, the 3.2mm and 3.7mm diameter stents demonstrated they had the most balanced composition of HWSS and LWSS areas. Considering the inconclusive data regarding the more adverse option between HWSS and LWSS, this suggests that selecting stents within this diameter range may provide the most sound stent design in terms of stable radial stiffness and hemodynamic properties. However, due to the unique lumen diameters of the average human, truly optimal stent diameters are yet to be conclusive. In selecting a stent within this range, underexpansion or overexpansion may occur depending on the patient’s lumen diameter, causing greater risk of adverse clinical outcomes despite their favourable attributes. As only quantitative data has been provided, it is recommended to perform more in-vivo experiments – ideally within patients of similar lumen diameters – in testing the aforementioned stent ranges.

In analysing the evidence between stent parameters and stent performance, a few parameters indicated a positive correlation. In particular, stent cross sections, where circular cross sectional stents were recommended via the optimisation algorithm for smaller stent diameters, whilst rectangular cross sectional stents were recommended for the larger stent diameters. As circular cross sectional struts have been associated with lower areas of LWSS [43] and rectangular cross sectional struts are favoured because of their higher surface area and strength, it is likely that a rectangular cross section was deemed necessary for larger stent diameters to maintain satisfactory radial strength. However, as low LWSS areas have also been correspondent with lower stent diameters, these data points are in direct conflict and hence may contribute towards skewing the values obtained in Figure 31. Similarly, despite the strength advantages of rectangular cross sectional stents, due to the structurally weaker composition of larger stent diameters, the radial stiffness values observed in the FEA graphs may also appear less detrimental than actuality.

This study aimed to provide insight into the effects on stent mechanical and hemodynamic performance by varying common commercially adopted stent diameters. Primarily, the radial stiffness was shown to largely

decrease with greater stent diameters, and depending on the density of the material, may potentially lead to large discrepancies. The percentage of LWSS and HWSS areas were also largely correlated with stent diameters, which may provide for useful statistics in the selection of stent diameters when considering hemodynamic performance.

#### **4.5. Future Work**

The possibilities and combinations in stent performance and characteristics are copious, and hence – in addition to the data obtained in this thesis – many more options can be explored for future work. In particular, additional simulations involving stent materials should be considered. As only one stent design of ‘sopt4’ was considered for the different material types, it is likely that a greater diversity of results will be obtained, rather than the current linear trend shown. For example, materials such as nitinol or tantalum could be applied for the respective diameters, and are recommended due to their relatively distinguishing density values, and common application in stent research.

Furthermore, a greater range of stent diameters should also be investigated in future work – notably stents outside of the 3mm to 4mm range, and within the 3.2mm to 3.7mm range. This is due to the extremes of HWSS and LWSS areas noted at either end of the spectrum, and poses the question of whether this trend will continue for stents which are outside of this boundary. Similarly, due to the ‘ideal range’ within the 3.2mm and 3.7mm stent diameter range, stent diameters which receive low percentage areas of both HWSS and LWSS could potentially be discovered, which could further be optimized through customizing different stent parameters such as cell height and cross sectional shape. The number of optimized stents produced could also have been increased, allowing for more comparable samples between the stent diameters. Furthermore, an interesting element of the optimisation algorithm – the use of rectangular stents were favoured in larger diameters. This should be further investigated as to determine if this was a necessary adjustment due to the advantageous features of circular strutted stents in reducing LWSS levels.

As this report omitted the use of connectors, additional simulations may endeavour to consult the problem of invalid stent geometries. This was caused by clashing bodies of the connectors, and hence may require an alteration or revision of the geometry creation script.

As this thesis was also performed theoretically, realistic outcomes concerning ISR, ST and MI were not considered, and hence may be greatly improved by incorporating in-vivo experiments with future work. For more achievable outcomes, in-vitro testing may also be performed, and can be realised through 3D printing of select stent designs. By using a physical model, actual deformation values may be observed and compared with theoretical data points to confirm the accuracy of the simulations being generated. Hence,

a myriad of possible pathways may be explored for proceeding research, and would benefit from rectifying any gaps from the research performed in this thesis.

## 5. Conclusions

This thesis has provided a general overview of the intricacies involved in analysing stent performance, achieved through the multi-objective optimisation process of stent designs. Data was gathered primarily from literature review, peer review and original experimental research. This was performed through computational tools consisting of ANSYS, Matlab, and third party software Katana OnDemand. A focus was placed upon vessel calibre and stent diameters, of which the diameters ‘3mm’, ‘3.2mm’, ‘3.7mm’ and ‘4mm’ were computationally generated and analysed in regards to their performance in minimizing low TAWSS, high WSS, and maximizing radial stiffness. 19 unique stent geometries were constructed for each respective stent diameter, with identical stent parameters for every stent, with 9 stents employing rectangular cross sectional struts, and 10 stents employing circular cross sectional struts. These were iteratively optimized four times through the optimisation algorithm script, and used as reference against previous work conducted by Vanessa Luvio and Deepan Kumar.

Radial stiffness values were found to gradually drop as the stent diameter ranges increased, which is in agreement with the widely accepted notion in the field of physics that ‘smaller is stronger’ and similar experiments performed in the past. Furthermore, attributed to their higher density and mechanical strength, the L605 Cobalt Chromium material outperformed other commonly utilised materials in MP35N Cobalt Chromium, Platinum Chromium and Stainless Steel. However, due to the low amount of data points taken in its sampling, additional simulations should be performed to draw further conclusions.

Higher percentage areas of LWSS were found in larger stent diameters, whilst higher percentage areas of HWSS were found in smaller stent diameters. From literature examining the definite adverse effects of LWSS, smaller stent diameters are also instinctively more beneficial in handling hemodynamic flow. However, as in-vivo circumstances have not been accounted for, the theoretically superior characteristics of smaller stent diameters may be outweighed by clinical outcomes such as ISR.

Optimal levels of radial stiffness and WSS were also found in the range between 3.2mm and 3.7mm diameter stents, and hence indicates the potential in developing additional simulations to investigate possible geometries with optimal characteristics.

Overall, concrete quantitative conclusions have been formed from compiling the information presented in this thesis, and serves as a suitable baseline for future research to be conducted. Additional stent parameters – notably connectors – should be attempted for design integration, and practical assessments of optimized stent designs may be tested using in-vitro methods, such as stress tests of 3D printed stents.

Nonetheless, this data has provided useful input into the understanding of stent diameter its behaviour towards key objectives when exposed to specific circumstances, and will be beneficial to the development of future stent research and experimentation.

## References

### References

- [1] Mayo Clinic. 2021. Coronary angioplasty and stents - Mayo Clinic. [online] Available at: <<https://www.mayoclinic.org/tests-procedures/coronary-angioplasty/about/pac-20384761>> [Accessed 4 July 2021].
- [2] Golden Shutter Films. 2021. Percutaneous Coronary Intervention (PCI) — Golden Shutter Films. [online] Available at: <<https://rodnieoro.com/home/percutaneous-coronary-intervention-angioplasty>> [Accessed 5 April 2022].
- [3] Buccheri, D., Piraino, D., Andolina, G. and Cortese, B., 2016. Understanding and managing in-stent restenosis: a review of clinical data, from pathogenesis to treatment. [online] Available at: <<https://pubmed.ncbi.nlm.nih.gov/27867580/>> [Accessed 15 July 2021].
- [4] Huda Hamid, J., 2021. ‘Miracle stents’ - a future without restenosis. [online] PubMed Central (PMC). Available at: <<https://www.ncbi.nlm.nih.gov/pmc/articles/PMC2323487/>> [Accessed 3 July 2021].
- [5] Dehmer, G. and Smith, K., 2009. Drug-Eluting Coronary Artery Stents. [online] Aafp.org. Available at: <<https://www.aafp.org/afp/2009/1201/p1245.html>> [Accessed 10 July 2021].
- [6] Modi, K., Soos, M. and Mahajan, K., 2020. Stent Thrombosis. [online] Ncbi.nlm.nih.gov. Available at: <<https://www.ncbi.nlm.nih.gov/books/NBK441908/>> [Accessed 15 July 2021].
- [7] Circulation. 2015. Drug-Eluting Stent and Coronary Thrombosis. [online] Available at: <<https://www.ahajournals.org/doi/full/10.1161/CIRCULATIONAHA.106.675934>> [Accessed 4 July 2021].
- [8] Aung, S., Latt, H., Kyaw, K. and Roongsritong, C., 2018. An Interesting Case and Literature Review of a Coronary Stent Fracture in a Current Generation Platinum Chromium Everolimus-Eluting Stent. [online] Available at: <<https://www.ncbi.nlm.nih.gov/pubmed/29967699>> [Accessed 13 July 2021].
- [9] Circulation: Cardiovascular Interventions. 2018. Incidence and Clinical Impact of Stent Fracture After Everolimus-Eluting Stent Implantation. [online] Available at: <<https://www.ahajournals.org/doi/10.1161/CIRCINTERVENTIONS.112.969238>> [Accessed 18 July 2021].
- [10] Chinikar, M. and Sadeghipour, P., 2021. Coronary Stent Fracture: A Recently Appreciated Phenomenon with Clinical Relevance. [online] Available at: <<https://pubmed.ncbi.nlm.nih.gov/24720422>> [Accessed 26 July 2021].
- [11] Circulation: Cardiovascular Interventions. 2016. Comprehensive Intravascular Ultrasound Assessment of Stent Area and Its Impact on Restenosis and Adverse Cardiac Events in 403 Patients With Unprotected Left Main Disease. [online] Available at: <<https://www.ahajournals.org/doi/10.1161/CIRCINTERVENTIONS.111.964643>> [Accessed 4 July 2021].
- [12] Mehrdad Taherioun, S., 2014. Stent underexpansion in angiographic guided percutaneous coronary intervention, despite adjunctive balloon post-dilatation, in drug eluting stent era. [online] PubMed Central (PMC). Available at: <<https://www.ncbi.nlm.nih.gov/pmc/articles/PMC4063511/>> [Accessed 15 July 2021].
- [13] LaDisa, J., Olson, L., Hettrick, D., Warltier, D., Kersten, J. and Pagel, P., 2005. Axial stent strut angle influences wall shear stress after stent implantation: analysis using 3D computational fluid dynamics models of stent foreshortening. [online] Available at: <<https://pubmed.ncbi.nlm.nih.gov/16250918>> [Accessed 19 July 2021].
- [14] Khosravi, A., Akbari, A., Bahreinizad, H., Salimi Bani, M. and Karimi, A., 2008. Optimizing through computational modeling to reduce dogboning of functionally graded coronary stent material. [online] Available at: <<https://pubmed.ncbi.nlm.nih.gov/28819891>> [Accessed 5 August 2021].

- [15] Lim, D., Cho, S., Park, W., Kristensson, A., Ko, J., Al-Hassani, S. and Kim, H., 2017. Suggestion of Potential Stent Design Parameters to Reduce Restenosis Risk driven by Foreshortening or Dogboning due to Non-uniform Balloon-Stent Expansion. [online] Available at: <<https://pubmed.ncbi.nlm.nih.gov/18437572>> [Accessed 28 July 2021].
- [16] Qiao, A. and Zhang, Z., 2021. Numerical Simulation of Vertebral Artery Stenosis Treated With Different Stents. [online] Available at: <<https://www.ncbi.nlm.nih.gov/pubmed/24337228>> [Accessed 12 July 2021].
- [17] Mortier, P., De Beule, M., Carlier, S., Van Impe, R., Verhegghe, B. and Verdonck, P., 2015. Numerical Study of the Uniformity of Balloon-Expandable Stent Deployment. [online] Available at: <<http://Numerical Study of the Uniformity of Balloon-Expandable Stent Deployment>> [Accessed 7 July 2021].
- [18] Jenei, C., Balogh, E., Szabó, G., Dézsi, C. and Kőszegi, Z., 2018. Wall shear stress in the development of in-stent restenosis revisited. A critical review of clinical data on shear stress after intracoronary stent implantation. [online] Available at: <[https://journals.viamedica.pl/cardiology\\_journal/article/view/44554](https://journals.viamedica.pl/cardiology_journal/article/view/44554)> [Accessed 16 July 2021].
- [19] Eshtehardi, P., Brown, A., Bhargava, A., Costopoulos, C., Hung, O., Corban, M., Hosseini, H., Gogas, B., Giddens, D. and Samady, H., 2017. High wall shear stress and high-risk plaque: an emerging concept. [online] Available at: <<https://pubmed.ncbi.nlm.nih.gov/28074425>> [Accessed 8 July 2021].
- [20] Lauric, A., Hippelheuser, J. and Malek, A., 2015. Induction of aneurysmogenic high positive wall shear stress gradient by wide angle at cerebral bifurcations, independent of flow rate. [online] Available at: <<https://pubmed.ncbi.nlm.nih.gov/30095336>> [Accessed 12 July 2021].
- [21] Bedoya, J., Meyer, C., Timmins, L., Moreno, M. and Moore, J., 2006. Effects of Stent Design Parameters on Normal Artery Wall Mechanics. [online] Available at: <<https://asmedigitalcollection.asme.org/biomechanical/article-abstract/128/5/757/466381/Effects-of-Stent-Design-Parameters-on-Normal?redirectedFrom=fulltext>> [Accessed 23 July 2021].
- [22] Pinto, S. and Campos, J., 2016. Numerical study of wall shear stress-based descriptors in the human left coronary artery. [online] Available at: <<https://pubmed.ncbi.nlm.nih.gov/26883291>> [Accessed 25 July 2021].
- [23] Iqbal, J., Gunn, J. and Serruys, P., 2013. Coronary stents: historical development, current status and future directions. [online] Available at: <<https://pubmed.ncbi.nlm.nih.gov/23532779>> [Accessed 17 July 2021].
- [24] Uspharmacist.com. 2021. Drug-Eluting Stents. [online] Available at: <<https://www.uspharmacist.com/article/drug-eluting-stents>> [Accessed 5 July 2021].
- [25] Navarese, E., Kowalewski, M., Kandzari, D., Lansky, A., Górný, B., Kołtowski, Ł., Waksman, R., Berti, S., Musumeci, G., Limbruno, U., van der Schaaf, R., Kelm, M., Kubica, J. and Suryapranata, H., 2014. First-generation versus second-generation drug-eluting stents in current clinical practice: updated evidence from a comprehensive meta-analysis of randomised clinical trials comprising 31 379 patients. [online] Available at: <<https://pubmed.ncbi.nlm.nih.gov/25332803>> [Accessed 16 July 2021].
- [26] Watson, T., Webster, M., Ormiston, J., Ruygrok, P. and Stewart, J., 2017. Long and short of optimal stent design. [online] Available at: <<https://www.ncbi.nlm.nih.gov/pubmed/29118997>> [Accessed 17 July 2021].
- [27] Wei, L., Leo, H., Chen, Q. and Li, Z., 2019. Structural and Hemodynamic Analyses of Different Stent Structures in Curved and Stenotic Coronary Artery. [online] Available at: <<https://www.frontiersin.org/articles/10.3389/fbioe.2019.00366>> [Accessed 14 July 2021].

- [28] Beier, S., Ormiston, J., Webster, M., Cater, J., Norris, S., Medrano-Gracia, P., Young, A. and Cowan, B., 2016. Hemodynamics in Idealized Stented Coronary Arteries: Important Stent Design Considerations. [online] Available at: <<https://pubmed.ncbi.nlm.nih.gov/26178872>> [Accessed 10 July 2021].
- [29] Kastrati, A., Mehilli, J., Dirschinger, J., Dotzer, F., Schühlen, H., Neumann, F., Fleckenstein, M., Pfaffert, C., Seyfarth, M. and Schömig, A., 2001. Intracoronary Stenting and Angiographic Results. [online] Available at: <<https://pubmed.ncbi.nlm.nih.gov/11401938>> [Accessed 2 July 2021].
- [30] Iantorno, M., Lipinski, M., Garcia-Garcia, H., Forrester, B., Rogers, T., Gajana, D., Buchanan, K., Torguson, R., Weintraub, W. and Waksman, R., 2018. Meta-Analysis of the Impact of Strut Thickness on Outcomes in Patients With Drug-Eluting Stents in a Coronary Artery. [online] Available at: <<https://pubmed.ncbi.nlm.nih.gov/30292330>> [Accessed 27 June 2021].
- [31] Kawamoto, H., Panoulas, V., Sato, K., Miyazaki, T., Naganuma, T., Sticchi, A., Figini, F., Latib, A., Chieffo, A., Carlino, M., Montorfano, M. and Colombo, A., 2015. Impact of Strut Width in Periprocedural Myocardial Infarction. [online] Available at: <<https://www.sciencedirect.com/science/article/pii/S1936879815004872>> [Accessed 14 July 2021].
- [32] Pant, S., Bressloff, N. and Limbert, G., 2012. Geometry parameterization and multidisciplinary constrained optimization of coronary stents. [online] Available at: <<https://pubmed.ncbi.nlm.nih.gov/21373889/>> [Accessed 9 July 2021].
- [33] Mauri, L., O'Malley, A., Cutlip, D., Ho, K., Popma, J., Chauhan, M., Baim, D., Cohen, D. and Kuntz, R., 2004. Effects of stent length and lesion length on coronary restenosis. [online] Available at: <<https://pubmed.ncbi.nlm.nih.gov/15165911/>> [Accessed 9 July 2021].
- [34] Kang, S., Ahn, J., Song, H., Kim, W., Lee, J., Park, D., Yun, S., Lee, S., Kim, Y., Lee, C., Mintz, G., Park, S. and Park, S., 2011. Comprehensive Intravascular Ultrasound Assessment of Stent Area and Its Impact on Restenosis and Adverse Cardiac Events in 403 Patients With Unprotected Left Main Disease. [online] Available at: <<https://pubmed.ncbi.nlm.nih.gov/22045969/>> [Accessed 19 July 2021].
- [35] Chiastra, C. and Migliavacca, F., 2021. Modeling of Blood Flow in Stented Coronary Arteries. [online] Available at: <<https://www.sciencedirect.com/science/article/pii/B9780124080775000122>> [Accessed 24 July 2021].
- [36] Plitt, A., Claessen, B., Sartori, S., Baber, U., Chandrasekhar, J., Aquino, M., Vijay, P., Elsayed, S., Kovacic, J., Sweeny, J., Barman, N., Moreno, P., Krishnan, P., Demopoulos, A., Dangas, G., Kini, A., Mehran, R. and Sharma, S., 2020. Impact of stent diameter on outcomes following percutaneous coronary intervention with second-generation drug-eluting stents: Results from a large single-center registry. [online] Available at: <<https://pubmed.ncbi.nlm.nih.gov/31490029/>> [Accessed 25 July 2021].
- [37] Gundert, T., Marsden, A., Yang, W., Marks, D. and LaDisa, Jr, J., 2012. Identification of Hemodynamically Optimal Coronary Stent Designs Based on Vessel Caliber. [online] Available at: <<https://pubmed.ncbi.nlm.nih.gov/22547450/>> [Accessed 4 July 2021].
- [38] Iannaccone, M., Gatti, P., Barbero, U., Bassignana, A., Gallo, D., Benedictis, M., Helft, G., Morbiducci, U., Doronzo, B. and D'Ascenzo, F., 2020. Impact of strut thickness and number of crown and connectors on clinical outcomes on patients treated with second-generation drug eluting stent. [online] Available at: <<https://pubmed.ncbi.nlm.nih.gov/30980471/>> [Accessed 7 July 2021].
- [39] Foin, N., Sen, S., Allegria, E., Petraco, R., Nijjer, S., Francis, D., Di Mario, C. and Davies, J., 2013. Maximal expansion capacity with current DES platforms: a critical factor for stent selection in the treatment of left main bifurcations?. [online] Available at: <<https://pubmed.ncbi.nlm.nih.gov/23086760/>> [Accessed 24 July 2021].

- [40] Pant, S., Bressloff, N., Forrester, A. and Curzen, N., 2010. The Influence of Strut-Connectors in Stented Vessels: A Comparison of Pulsatile Flow Through Five Coronary Stents. [online] Available at: <<https://pubmed.ncbi.nlm.nih.gov/20177782>> [Accessed 18 July 2021].
- [41] Shen, X., Xie, Z., Deng, Y. and Ji, S., 2021. Effects of Metal Material Stent Design Parameters on Longitudinal Stent Strength. [online] Available at: <<https://www.scientific.net/KEM.723.299>> [Accessed 20 July 2021].
- [42] Watson, T., Webster, M., Ormiston, J., Ruygrok, P. and Stewart, J., 2017. Long and short of optimal stent design. [online] Available at: <<https://www.ncbi.nlm.nih.gov/pubmed/29118997>> [Accessed 11 July 2021].
- [43] Jiang, Y., Zhang, J. and Zhao, W., 2016. Influence of strut cross-section of stents on local hemodynamics in stented arteries. [online] Available at: <<https://cjme.springeropen.com/articles/10.3901/CJME.2016.0125.013>> [Accessed 18 July 2021].
- [44] Levy, E. and Levy, Y., 2016. Comparing the Effect of Stent Geometry on Blood Flow Rate of Curved Coronary Artery Stenosis | Journal of Emerging Investigators. [online] Emerginginvestigators.org. Available at: <<https://www.emerginginvestigators.org/articles/comparing-the-effect-of-stent-geometry-on-blood-flow-rate-of-curved-coronary-artery-stenosis>> [Accessed 28 July 2021].
- [45] Jiménez, J. and Davies, P., 2009. Hemodynamically Driven Stent Strut Design. [online] Available at: <<https://pubmed.ncbi.nlm.nih.gov/19472055>> [Accessed 30 July 2021].
- [46] Zhou, F., Liu, Y., Ge, P., Chen, Z., Ding, X., Liu, J., Jia, Q., An, F., Li, L., Wang, L., Ma, W., Yang, Z. and Jia, E., 2017. Coronary Artery Diameter is Inversely Associated with the Severity of Coronary Lesions in Patients Undergoing Coronary Angiography. [online] Available at: <<https://pubmed.ncbi.nlm.nih.gov/28977790/>> [Accessed 10 April 2022].
- [47] Commons.wikimedia.org. 2007. File:Coronary.pdf - Wikimedia Commons. [online] Available at: <<https://commons.wikimedia.org/wiki/File:Coronary.pdf>> [Accessed 12 April 2022].
- [48] Circulation: Cardiovascular Interventions. 2009. Effect of Length and Diameter of Drug-Eluting Stents Versus Bare-Metal Stents on Late Outcomes. [online] Available at: <<https://www.ahajournals.org/doi/10.1161/circinterventions.108.805630>> [Accessed 13 April 2022].
- [49] Kitahara, H., 2017. Impact of Stent Size Selection on Acute and Long-Term Outcomes After Drug-Eluting Stent Implantation in De Novo Coronary Lesions. [online] Circulation: Cardiovascular Interventions. Available at: <<https://www.ahajournals.org/doi/10.1161/CIRCINTERVENTIONS.116.004795>> [Accessed 13 April 2022].
- [50] Stiehm, M., Wüstenhagen, C., Siewert, S., Ince, H., Grabow, N. and Schmitz, K., 2017. Impact of strut dimensions and vessel caliber on thrombosis risk of bioresorbable scaffolds using hemodynamic metrics. [online] Available at: <<https://pubmed.ncbi.nlm.nih.gov/29933242>> [Accessed 13 April 2022].
- [51] Martin, D. and Boyle, F., 2011. Computational structural modelling of coronary stent deployment: a review. [online] Available at: <<https://www.ncbi.nlm.nih.gov/pubmed/20589544>> [Accessed 27 July 2021].
- [52] Hsiao, H., Chiu, Y., Lee, K. and Lin, C., 2012. Computational modeling of effects of intravascular stent design on key mechanical and hemodynamic behavior. [online] Available at: <<https://www.sciencedirect.com/science/article/abs/pii/S001044851200070X>> [Accessed 20 July 2021].
- [53] Martin, D. and Boyle, F., 2011. Computational structural modelling of coronary stent deployment: a review. [online] Available at: <<https://www.ncbi.nlm.nih.gov/pubmed/20589544>> [Accessed 20 July 2021].



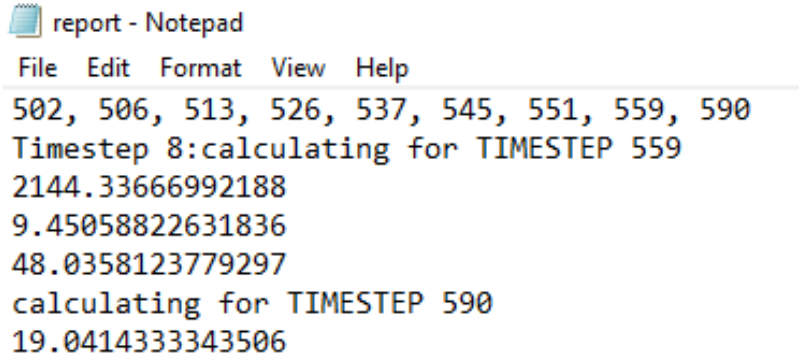
- [54] Schiavone, A. and Zhao, L., 2015. A study of balloon type, system constraint and artery constitutive model used in finite element simulation of stent deployment. [online] Link.springer.com. Available at: <<https://link.springer.com/content/pdf/10.1186/s40759-014-0002-x.pdf>> [Accessed 27 July 2021].
- [55] Azaouzi, M., Makradi, A. and Belouettar, S., 2012. Deployment of a self-expanding stent inside an artery: A finite element analysis. [online] Available at: <<https://www.sciencedirect.com/science/article/pii/S0261306912003202>> [Accessed 25 July 2021].
- [56] De Santis, G., De Beule, M., Van Canneyt, K., Segers, P., Verdonck, P. and Verhegghe, B., 2011. Full-hexahedral structured meshing for image-based computational vascular modeling. [online] Available at: <<https://pubmed.ncbi.nlm.nih.gov/21763174/>> [Accessed 26 July 2021].
- [57] Thrinayan, M., 2019. Patient Specific Coronary Stent Designing and its Computational Analysis using Ansys. [online] Iopscience.iop.org. Available at: <<https://iopscience.iop.org/article/10.1088/1742-6596/1362/1/012052/pdf>> [Accessed 27 July 2021].
- [58] Hsiao, H., Chiu, Y., Lee, K. and Lin, C., 2012. Computational modeling of effects of intravascular stent design on key mechanical and hemodynamic behavior. [online] Available at: <<https://www.sciencedirect.com/science/article/pii/S001044851200070X>> [Accessed 18 July 2021].
- [59] Eshghi, N., Hojjati, M., Imani, M. and Goudarzi, A., 2011. Finite Element Analysis of Mechanical Behaviors of Coronary Stent. [online] Available at: <<https://www.sciencedirect.com/science/article/pii/S1877705811006941>> [Accessed 23 July 2021].
- [60] Lally, C., Dolan, F. and Prendergast, P., 2005. Cardiovascular stent design and vessel stresses: a finite element analysis. [online] Available at: <<https://pubmed.ncbi.nlm.nih.gov/15958213/>> [Accessed 30 July 2021].
- [61] Umer, M., Najabat, M., Mubashar, A. and Mir, M., 2019. Computational modeling of balloon-expandable stent deployment in coronary artery using the finite element method. [online] Doaj.org. Available at: <<https://doaj.org/article/d4b1b3592e6844d98e6362c9684c75e8>> [Accessed 16 July 2021].
- [62] Wang, Q., Fang, G., Zhao, Y., Wang, G. and Cai, T., 2017. Computational and experimental investigation into mechanical performances of Poly-L-Lactide Acid (PLLA) coronary stents. [online] Available at: <<https://www.sciencedirect.com/science/article/pii/S1751616116303010>> [Accessed 23 July 2021].
- [63] Lotfi, A., Simmons, A. and Barber, T., 2016. Evaluation of Different Meshing Techniques for the Case of a Stented Artery. [online] Available at: <<https://pubmed.ncbi.nlm.nih.gov/26784359/>> [Accessed 22 July 2021].
- [64] Eshghi, N., Hojjati, M., Imani, M. and Goudarzi, A., 2011. Finite Element Analysis of Mechanical Behaviors of Coronary Stent. [online] Available at: <<https://www.sciencedirect.com/science/article/pii/S1877705811006941>> [Accessed 19 July 2021].
- [65] Gharleghi, R., Wright, H., Khullar, S., Liu, J., Ray, T. and Beier, S., 2019. Advanced Multi-objective Design Analysis to Identify Ideal Stent Design. [online] Available at: <[https://link.springer.com/chapter/10.1007/978-3-030-33327-0\\_23](https://link.springer.com/chapter/10.1007/978-3-030-33327-0_23)> [Accessed 27 July 2021].
- [66] Bostonscientific.com. 2018. PROMUS Elite. [online] Available at: <[https://www.bostonscientific.com/content/dam/bostonscientific/Interventional%20Cardiology/portfolio-group/Stents/promus-elite/library/IC-555505-AA\\_US\\_Promus\\_ELITE\\_Spec\\_Sheet\\_FINAL.pdf](https://www.bostonscientific.com/content/dam/bostonscientific/Interventional%20Cardiology/portfolio-group/Stents/promus-elite/library/IC-555505-AA_US_Promus_ELITE_Spec_Sheet_FINAL.pdf)> [Accessed 8 April 2022].

- [67] Medtronic.com. 2011. Bare Metal Coronary Stents. [online] Available at: <[https://www.medtronic.com/content/dam/medtronic-com/products/coronary/stents/integrity-bare-metal/documents/Integrity\\_RX\\_Catalog.pdf?bypassIM=trueStents/promus-elite/library/IC-555505-AA\\_US\\_Promus\\_ELITE\\_Spec\\_Sheet\\_FINAL.pdf](https://www.medtronic.com/content/dam/medtronic-com/products/coronary/stents/integrity-bare-metal/documents/Integrity_RX_Catalog.pdf?bypassIM=trueStents/promus-elite/library/IC-555505-AA_US_Promus_ELITE_Spec_Sheet_FINAL.pdf)> [Accessed 13 April 2022].
- [68] Luvio, V., Multi-objective optimisation of coronary stents, 2020 [Accessed 10 June 2021]
- [69] Kumar, A., 2019. Design Methodology of a Balloon Expandable Polymeric Stent. [online] Journal of Biomedical Engineering and Medical Devices. Available at: <<https://www.longdom.org/open-access/design-methodology-of-a-balloon-expandable-polymeric-stent-44132.html>> [Accessed 6 April 2022].
- [70] Zhao, S. and Gu, L., 2011. Assessment of Shape Memory Alloy Stent Deployment in a Stenosed Artery. [online] ResearchGate. Available at: <[https://www.researchgate.net/publication/231111449\\_Assessment\\_of\\_Shape\\_Memory\\_Alloy\\_Stent\\_Deployment\\_in\\_a\\_Stenosed\\_Artery](https://www.researchgate.net/publication/231111449_Assessment_of_Shape_Memory_Alloy_Stent_Deployment_in_a_Stenosed_Artery)> [Accessed 11 April 2022].
- [71] LaDisa, J., 2004. Stent design properties and deployment ratio influence indexes of wall shear stress: a three-dimensional computational fluid dynamics investigation within a normal artery | Journal of Applied Physiology. [online] Journal of Applied Physiology. Available at: <[https://journals.physiology.org/doi/full/10.1152/japplphysiol.01329.2003?rfr\\_dat=cr\\_pub++0pubmed&url\\_ver=Z39.88-2003&rfr\\_id=ori%3Arid%3Aacrossref.org](https://journals.physiology.org/doi/full/10.1152/japplphysiol.01329.2003?rfr_dat=cr_pub++0pubmed&url_ver=Z39.88-2003&rfr_id=ori%3Arid%3Aacrossref.org)> [Accessed 15 April 2022].

## Appendices

### 5.1. Appendix A

The following figures denotes the CFD output created from the script. The 3<sup>rd</sup> line denotes the flow rate, 4<sup>th</sup> line the LWSS, and 5<sup>th</sup> line the HWSS.



```
report - Notepad
File Edit Format View Help
502, 506, 513, 526, 537, 545, 551, 559, 590
Timestep 8:calculating for TIMESTEP 559
2144.33666992188
9.45058822631836
48.0358123779297
calculating for TIMESTEP 590
19.0414333343506
```

Figure 33 - CFD output script

The following figures denotes the optimisation algorithm used, and the corresponding layout.

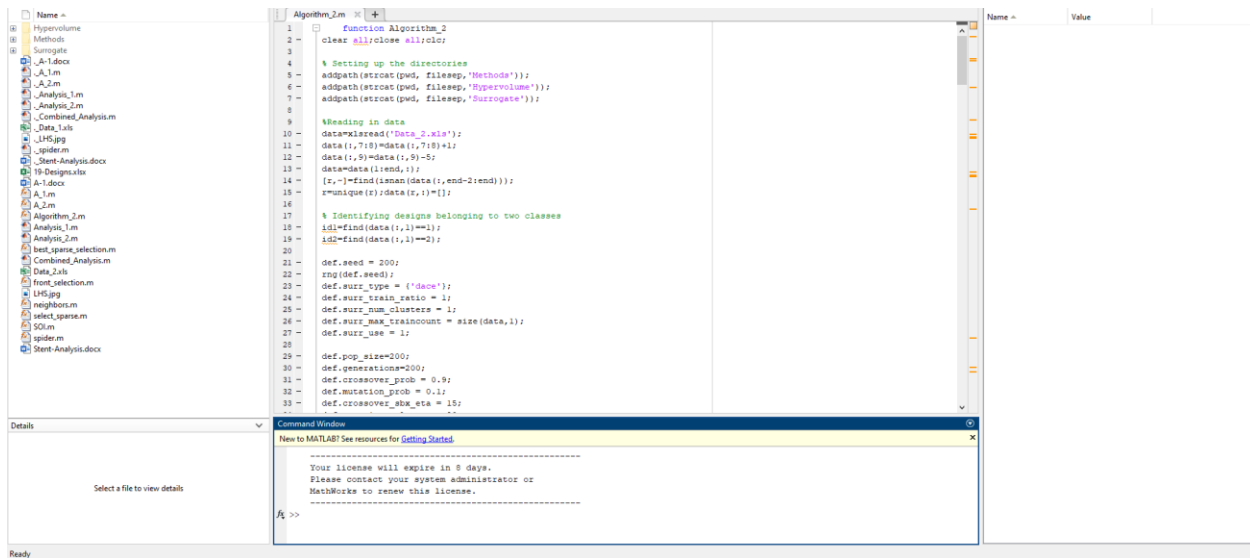


Figure 34 - MATLAB optimisation algorithm UI